POLITECNICO DI TORINO

Master's Degree in Biomedical Engineering

Politecnico di Torino

Master's Degree Thesis

Computational modeling of the cellular mechanism of Alzheimer's disease initiation due to tau protein hyperphosphorylation

Supervisors

Prof. Jack TUSZYNSKI

Candidate

Noemi MARGARITI

October 2023

Summary

Alzheimer's Disease (AD) is the most common form of dementia and one of the most impactful neurodegenerative diseases. Among several hypothesis of what could trigger the disease, the one investigated in this work is the Tau hypothesis. According to this, AD is triggered by an abnormal hyperphosphorylation of the protein tau, causing a detachment of the protein from microtubules (MTs) and consequent loss of stabily, leading so to their disruption and neuronal death.
In addition, studies have found a correlation between tau hyperphosphorylation and temperature that can vary the activity of kinases and phosphatases.
More in-depth, in this work our objective is to develop and explore a computational model of the cellular mechanism of the disease initiation due to tau protein hyperphosphorylation.

Acknowledgements

I would like to express my gratitude to Professor Tuszynski for his helpful contributions and for the opportunity he gave me.

And also to my family and friends, for supporting me in this journey through both easy and difficult moments.

Table of Contents

Acronyms

Aβ
: β-Amyloid

AD
: Alzheimer's Disease

APP
: Amyloid precursor protein

CaMKII
: Calcium/calmodulin-dependent protein kinase II

CDK1
: Cyclin-dependent kinase 1

CNS
: Central nervous system

GSK3
: Glycogen synthase kinase 3

HD
: Huntington's disease

IDP
: Intrinsically disordered protein

MAP
: Microtubule-associated protein

MTs

Microtubules

MTBD

Microtubule-binding domain

NFTs

Neurofibrillary tangles

ODE

Ordinary differential equation

PD

Parkinson's disease

PHFs

Paired helical filaments

PDE

Partial differential equation

PDPK

Proline-directed protein kinases

PP2A

Protein phosphatase 2A

PRD

Proline-rich domain

TPM

Transcripts par million

Chapter 1

Biological Background

1.1 Alzheimer's Disease

Alzheimer's disease (AD) is a neurodegenerative disease first described in 1907 by Aloise Alzheimer and, among other forms of dementia, it's considered the most common, accounting for up to 70% of cases. Clinical manifestation includes memory loss and cognitive decline, alongside behavioral dysfunction leading to an impairment of daily functions.

Depending on the severity of the histopathological alterations and the cognitive decline, the progress of the disease is classified in four phases: preclinical, mild, moderate and late-stage[1].

The neuronal loss and nerve cell atrophy typical of AD are accompanied by the distribution of two other structures: the β**-Amyloid** ($A\beta$) plaques[2] and the **neurofibrillary tangles** (NFT)[3]. These are considered the major hallmarks of AD and are the subjects of the two main hypothesis, along with others, on how the disease pathologically evolves.

β-Amyloid plaques consist of fibrils formed by the $A\beta$ peptides, which are composed by the sequential cleavage of transmembrane protein known as Amyloid Precursor Protein (APP) by β-secretase and γ-secretase. The predominant forms

of $A\beta$ peptide are the variants $A\beta_{1-40}$ and $A\beta_{1-42}$, and the latter is believed to be more citotoxic than the former[4]. The Amyloid Aggregation Process occurs in three phases: nucleation, elongation and stationary phase. Firstly, oligomeric $A\beta$ aggregates to form a nucleus, which can draw other monomers, then, as the fibrils grow, they can shatter, producing new aggregation-prone species to elongate the fibrils. When almost all free monomer is in a fibrillar form, the aggregates achieve a dynamic balance[5, 6, 7]. Recently, the Amyloid Hypothesis was questioned as has come to light some data falsification in the works on which the hypothesis was based on[8].

The second hypothesis regards the neuronal protein tau, whose role focuses on promoting microtubules (MTs) assembly and their stability depends on its degree of phosphorylation. An abnormal hyperphosphorylation of tau protein leads to the detachment of the protein from MTs, causing their disruption, and, consequently, it starts accumulating as intraneuronal tangles of paired helical filaments (PHF), twisted ribbons and or straight filaments, which are considered not only an hallmark lesion of AD, but also for other neurodegenerative disorders called tauopathies as Huntington's disease (HD), Parkinson's disease (PD) and Fronto-temporal dementia[9].

One of the possible causes that leads to tau hyperphosphorylation seems to be the dysregulation of the enzymes kinase and phosphatase. One of the pieces of evidence supporting this theory is that the levels of protein tau in the brain directly correlate to the severity of the disease, and a similar correlation is not observed for the $A\beta$. On the contrary, amyloid imaging lately has shown that in the brain of elderly non-demented patients, the distribution of β-Amyloid plaques is sometimes as extensive as that of AD patients suggesting that $A\beta$ deposition is a consequence of aging, and has no direct relation with the onset of the disease[9]. In light of it, it seems that the progression of AD is strongly associated with tau pathology,

considering that tau abnormalities cause accumulation of tau and degeneration of neurons, rather than $A\beta$ amyloid accumulation.

1.2 Tau Protein

1.2.1 Structure

Tau protein is a microtubule-associated protein (MAP) that is encoded by the MAPT gene, located on chromosome 17. Structurally, this protein is divided in several functional domains, depending on the length of the isoform: **N-terminal projection domain**, a **proline-rich domain** (PRD), a **microtubule binding domain** (MTBD), consisting in four partially repeated sequences (R1, R2, R3, R4), and a **C-terminal domain**[10].

In the Central Nervous System (CNS), tau protein is mostly found in the axonal compartment translated in six tau isoforms (0N3R, 0N4R, 1N3R, 1N4R, 2N3R, 2N4R), whose range varies from 352 to 441 amino acid residues and differ by having zero (0N), one (1N) or two amino-terminal (2N) insert and three (3R) or four (4R) microtubule-binding repeat sequences (**Figure 1.1**).

Tau protein is also subjected to several post-translational modifications, including phosphorylation, isomerisation, glycation, nitration, acetylation, oxidation and others, meaning that different tau-binding molecules share the same regulatory property of post-translational modifications, such as protein kinases and phosphatases[11].

Furthermore, tau protein is also considered an intrinsically disordered protein (IDP) and the modifications the processes mentioned would apply could promote new conformational changes in secondary structure that could facilitate the appearance of α-helix or β-sheet regions[12]. Among the possible modifications mentioned, the

most common and impactful between these processes is phoshorylation, as tau protein contains approximately 85 phosphorylation sites.

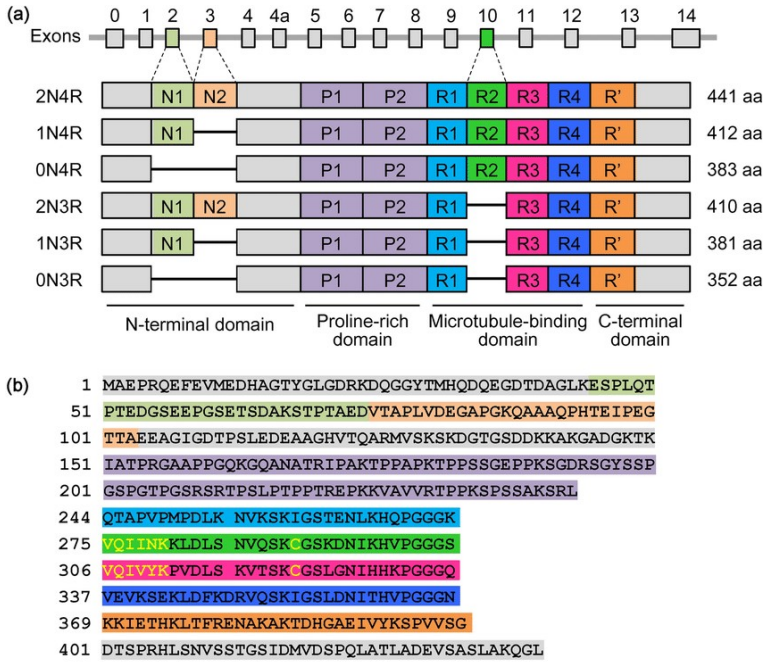

Figure 1.1: Primary structure of tau protein. a) Human MAPT gene encodes six tau isoforms showing the N-terminal inserts, two proline rich regions, the four MT-binding repeats and the C-terminal region. b) Amino acid sequence of 2N4R tau isoform. Individual region is indicated by the same color as in (a)[13]

1.2.2 Tau Pathology

As mentioned above, tau protein promotes and regulates its binding activity to MTs, their assembly and the maintenance of their stability. Under pathological conditions, conformational changes occur to the normal structure of tau, causing an increase of the protein in an hyperphosphorylated state, thus leading to the loss of tau's biological capacities.

It has been demonstrated that, in control brains, tau presents 2-3 mol P/mol tau,

while in Alzheimer's brains it was found up to 3-4 fold more hyperphosphorylated, with a concentration of $8PO_4$/mol.

In AD and other tauopathies, hyperphosphorylated tau induces MTs to disassemble and starts aggregating as PHF, twisted ribbons or straight filaments, which are referred to as NFTs if they are formed in neuronal cell bodies. Moreover, these pathological inclusions present all of the six tau isoforms in their hyperphosphorylated state[14].

Another form of abnormally hyperphosphorylated tau that can be found in AD is as non-fibrillized form in the cytosol, which, contrary to the one present in NFTs, does not interact with tubulin/MTs but instead sequesters normal tau, MAP1 and MAP2, causing inhibition and disassembly of MTs in vitro.

All this information and the studies behind demonstrate the significant involvement of abnormal hyperphosphorylation in neurofibrillary degeneration. And for this reason, there are many studies in progress focusing on tau as a target for therapy. The principal strategies[15] can be summarized as:

1. inhibition of abnormal tau hyperphosphorylation through modulation of specific protein kinases

2. induction of tau aggregates disassembly by using compounds like Methylene blue, Antharaquinones, etc.

3. stimulation of MTs stabilizing molecules with Taxol and Taxol-derived compounds

4. triggering of intracellular clearance pathways such as the ubiquitin-proteasome and/or autophagic system

5. tau immunotherapy

6. antiinflammatory therapy.

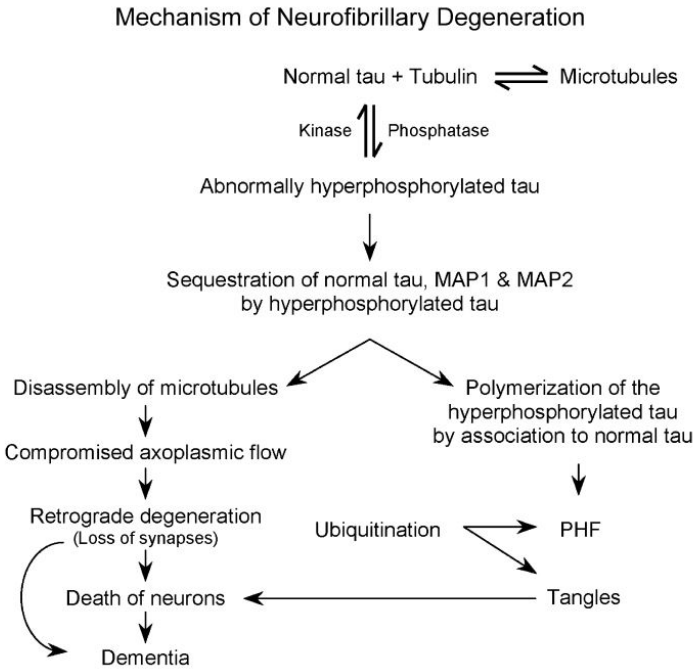

Figure 1.2: Mechanism of neurofibrillary degeneration.[14]

1.2.3 Kinases and Phosphatases

To investigate the role of tau protein and its hyperphosphorylated state in the disease, several studies have been conducted to get a clearer view on which kinases and phosphatases are involved in tau phosphorylation process.

Kinases and phosphatases are enzymes catalysing the transfer of phosphate between their substrates: the first ones catalyse the transfer of phosphate groups from ATP (or GTP) to its protein substrates, while the second ones catalyse the transfer

of the phosphate from a phosphoprotein to a water molecule. Even though both groups of enzymes are phosphotransferases, they catalyse opposing reactions to modulate the structures and functions of many cellular proteins[16].

Currently, several kinases have been identified and, moreover, they have been classifies in **proline-directed protein kinases** (PDPKs), that include MAP kinase, GSK3, cdk-1, cdk-2 and cdk-5, and **non-PDPKs** as PKA, CaMKII, CK-1 and CK-2.

The kinase considered a major pathogenic factor of AD is **Glycogen synthase kinase 3** (GSK3), that can be found in the isoforms GSK3β and GSK3α *Fan et al.* They are both prolific in the Central Nervous System (CNS) and share about 80% sequence homology[17].

Some evidence shows that, in transgenic mice, an overexpression of GSK3β induces tau hyperphosphorylation and consequently neurodegeneration, but also an overexpression in cell lines leads to apoptotic cell death, suggesting that tau phosphorylation by GSK3β could be toxic. This phosphorylation process by GSK3β also occurs in 42 sites of tau, 29 of which result phosphorylated in AD brains.

Moreover, to increase the phosphorylation efficiency by GSK3, it has been shown that the process called *substrate priming*, consisting in a pre-phosphorylation by PKA, PKC or CK-2 augmented the subsequent phosphorylation by GSK3. Further studies made evident that PKA was the actual kinase strengthening the process.

In particular, GSK3 alone was capable to phosphorylate Ser-181, Ser-184, Ser-262 and Ser-400 whether, in combination with PKA, phosphorylates Ser-195, Ser-198, Ser-199, Ser-202, Thr-205, Thr-231, Ser-235 and Ser-262[18].

In AD patients, GSK3β co-localizes with NFT and the phosphorylated at Tyr-216 form of GSK3β increases in the frontal cortex of AD brains. Thus, GSK3β is a prospective therapeutic target for tauopathies as AD because of the rise in its activity in AD brains and its role in the acceleration of tau pathology[17].

Calcium/calmodulin-dependent protein kinase II (CaMKII) is another kinase associated with AD and, more specifically, is a large holoenzyme composed of a six-domains central hub linked to twelve kinase domains and it's present in 4 isozymes: α, β, γ and δ.

Among the sites in tau that can be phosphorylated, Ser-131, Ser-214, Ser-262, Ser-356, Ser-416 and Thr-135, Thr-212 are the locations where CaMKII phosphorylates tau, and five of them are also observed to be phosphorylated in AD brains, with a significant impact on the metabolism and toxicity of tau[19, 17].

Furthermore, studies on CaMKII highlighted its essential role for memory encoding and long-term potentiation[20].

Another protein kinase considered is **cyclin-dependent kinase 1** (cdk1), which seems to have a central role in modulating tau phosphorylation in G2/M phase. Indeed, the inhibition of its activity determined the arrest of cells in G2/M phase in presence of non-phosphorylated Tau.

Moreover, there isn't any evidence supporting a direct role for cdk1 in the phosphorylation process of tau, but it could be hypothesized the presence of an indirect mechanism[21].

On the other hand, phosphatases involved in tauopathies belong to the phosphoproteinphosphatase group and namely they are PP1, PP2A, PP2B and PP5. Analysis of their activities in healthy human brain showed a predominance of **PP2A** activity, approximately 71%, compared to the others, but when it comes to pathological conditions total phosphatase activity seems reduced by half with a decrease of 50%, 20%, and 20% for PP2A, PP1 and PP5 respectively hinting at the idea that in AD certain phosphatases have a significant role[22].

On the basis of have been said, many studies focused on kinases and phosphatases as potential drug target in the search of a cure for Alzheimer's disease, focusing on finding inhibitors for kinases or activators in case of phosphatases, but there

haven't been any positive results yet.

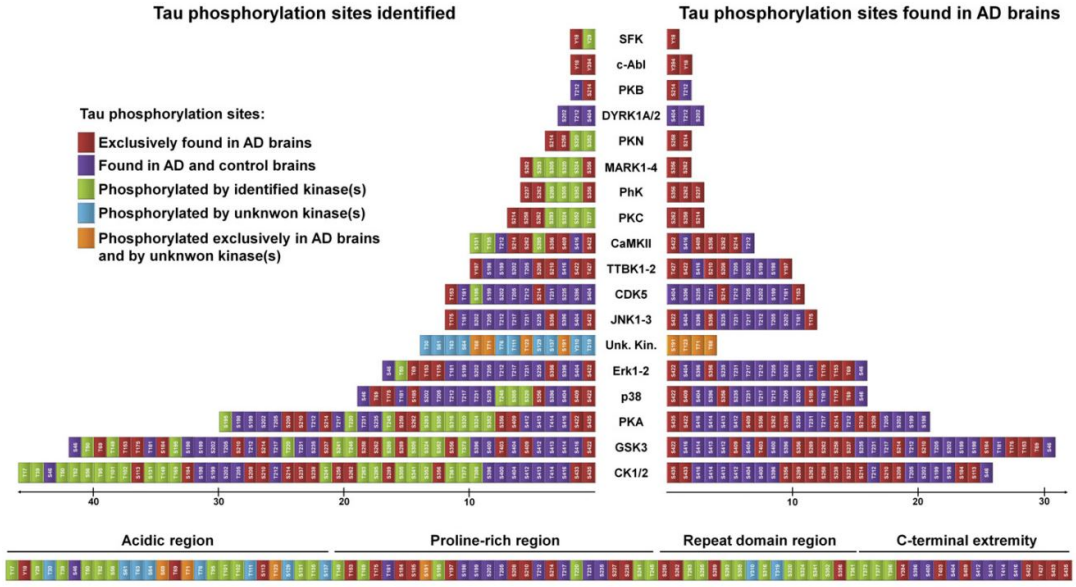

Figure 1.3: Pyramid of tau kinases. On the left, tau phosphorylation sites found phosphorylated by the considered kinase. On the right, tau phosphorylation sites found phosphorylated in AD brains.[17]

Chapter 2

Microtubules

2.1 Structure, organization and function

Microtubules are polymers shaped as hollow cylinders and structurally composed of 8nm long α- and β-tubulin heterodimers, confering them stiffness and length as well as a crucial role in the eukaryotic cell cytoskeleton, which, apart form MTs, is composed of actin and intermediate filaments. Usually, MTs have an outer diameter of 25 nm and an inner one between 11 and 15 nm, and as for length they can vary from 200nm to 25 μm (**Figure** 2.1).

Moreover, they consist in 13 strands of protofilaments of α- and β-tubulin dimers that connect laterally to form a tube structure, where α-subunits are exposed at one end of the MT and the β-subunits at the other one, defining so the structural polarity of the polymer.

This characteristic doesn't manifest exclusively at the two ends of the polymer, but also along its length and, as a matter of fact, this polarity is also recognized by motor proteins, which walk along the surface of the MT through the energy of ATP hydrolysis.

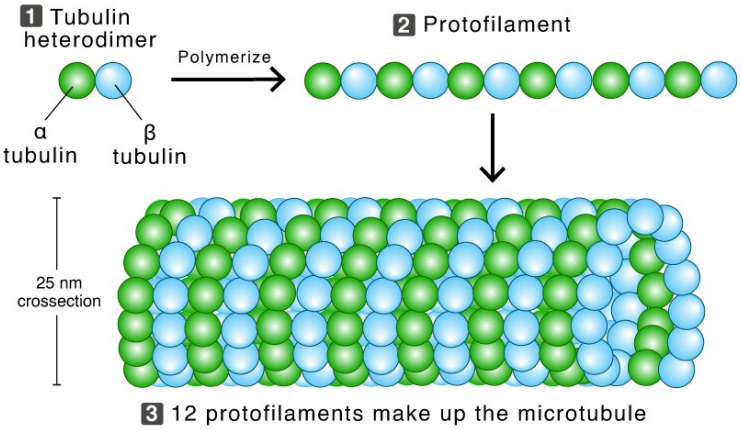

Figure 2.1: Structure of a microtubule.[23]

As a part of the cell cytoskeleton, MTs are found in all eukariotic cells, but it can be said that they are quite abundant in neuronal cells, mostly in axons and dendrites, where they arrange as paraxially aligned arrays, which are fundamental to help acquire and mantain particular morphologies. And other than a structural and supporting function, the presence of MTs in these cells is essential for early developmental stages of the cells, for the support of proteins and organelles transport within axons and dendrites in both directions and also for accommodating shape changes such as alterations in morphology that may correspond with cognitive plasticity even in old age[24].

2.2 Dynamic Instability

MTs are also extremely dynamic and this characteristic makes their structure hard to study, as they constantly undergo phases of assembly and disassembly.
The assembly process consist firstly in a nucleation phase, when MTs begin to grow from the centrosome with the help of guanosine triphosphate (GTP) molecule, a

strong energy source, bound to the α- and β- dimers.

Right after, an hydrolysis process begins resulting in MTs mostly made of GDP-tubulin, and then for the MTs core there is an addition of GTP-tubulin dimers to the MTs end where a GTP cap forms due to the delay between assembly and GTP hydrolysis at the tubulin inter-dimer interface. This cap has a stabilizing effect as its loss leads to MT depolymerization[25, 10, 26].

In summary, microtubules can grow as long as the heterodimers at the growing end remain bound with GTP, but in the case hydrolysis results fast enough the GTP cap dissolves and the MTs start collapsing, in a process called **catastrophe**. Through biochemical pumping, free GDP-tubulin can be converted to GTP-tubulin[27], and the MTs can undergo a process known as **rescue**, where they start growing again. This unique process of slow polymerization and fast depolymerization as a result of hydrolysis is called **dynamic instability**.

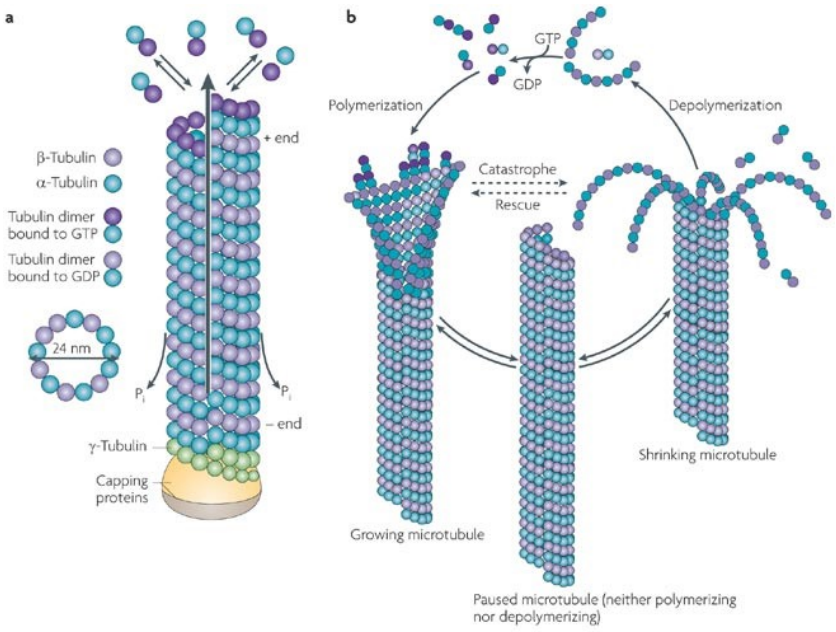

Figure 2.2: Process of dynamic instability.[28]

As mentioned in the previous chapter, tau is a microtubule-associated protein and as such its function is to stabilize MTs by decreasing the dissociation of tubulin at both MT ends, in order to decrease the chances of depolymerization. However, some studies led to the conclusion that not only tau is a stabilizer for MTs, but also a necessary protein to induce polymerization in the domain of MTs containing tyrosinated tubulin.
As documented, tau hyperphorylation, the consequent NFTs formation and decrease of tau-MT binding all correlate to neurodegeration. Phosphorylation at specific site as Ser-214, Ser-262 or Ser-356 seem to consistently decrease the affinity of tau for MTs, but the exact reasons or mechanisms by which hyperphosphorylated tau affects MT dynamics remain unclear.
What studies show is that hyperphosphorylated tau, when it starts aggregating, sequesters unphosphorylated tau from MT, causing loss of stability and consequent disruption[29].

2.2.1 Differences between *in vivo* and *in vitro* of dynamic instability

The behaviour of alternating phases of MTs growth and shortening previously described, can be observed and measured both in living cells and in vitro.
The characterization in vivo came later than the one in vitro, and the results highlighted that this behaviour differs from the two cases in several ways.
A first example is that the average growing rate of MTs is significantly higher in vivo than in vitro at similar tubulin concentration and, in living cells, several periods of pause, where MTs' length remain stable, were also observed, and, under steady-state conditions, some of these pauses could also be detected in vitro.
Furthermore, the transitions between phases are less frequent in vitro than in vivo.
All of these differences are determined not only from the experimental methods,

but also from cell types, stages of the cell cycle and presence and quantity of MAPs interacting with MTs[30].

2.3 Previous Work: mathematical models of MT dynamics

To describe the process of growth and shortening of MTs, several models, both computational and theoretical, have been developed, where the first ones aim to model the addition and subtraction of tubulin dimers, while the second ones to study the densities of growing and shortening MTs of different lengths over time.
One of the first works of theoretical models describing MT dynamics is from Dogterom and Leibler in 1993[31]. They describe growing and shortening length distributions of MTs through a partial differential equation (PDE) model considering MTs static only at the minus and non-interacting between each other.
The following equations define the model, focusing on the time evolution of probability densities of growing MTs, u and shrinking MTs, v

$$\frac{\partial u(x,t)}{\partial t} = -f_c u(x,t) + f_r v(x,t) - v_g \frac{\partial u(x,t)}{\partial x} \tag{2.1}$$

$$\frac{\partial v(x,t)}{\partial t} = f_c u(x,t) - f_r v(x,t) + v_s \frac{\partial v(x,t)}{\partial x} \tag{2.2}$$

where f_c, f_r, v_g and v_s are the four parameters usually describing dynamic instability, more specifically **frequencies of catastrophe and rescue**, and the average

speeds of growth and shortening, respectively. With this model, they were able to predict a transition between bounded and unbounded growth by varying the four parameters.

Considering the length distributions of MTs whenever $v_s f_c \geq v_g f_r$, the system doesn't reach a steady state and MTs lengths continue to increase linearly. On the other side, when $v_s f_c < v_g f_r$ the steady state for the length distribution is exponential. With an additional assumption that the dynamic parameters depend on GTP-tubulin concentration, c, the authors proposed that the threshold between bounded and unbounded growth can be reached by crossing some critical value $c{=}c_{cr}$.

In addition, from (2.1) and (2.2) it is possible to obtain useful parameters such as the mean velocity of the MT tip, calculated over several cycles of catastrophe and rescue

$$\overline{vel} = \frac{f_r v_g - f_c v_s}{f_r + f_c}$$

Moreover, the overall probability density p(x,t) = u(x,t) + v(x,t) approaches a time-dependent Gaussian distribution

$$p(x,t) = \frac{1}{\sqrt{4\pi D t}} \exp \frac{(x - \overline{vel}t)^2}{4Dt}$$

with D as a diffusion constant. This probability density also converges to a stationary exponential distribution with a mean length equal to

$$\overline{x} = \frac{v_g v_s}{f_c v_s - f_r v_g}$$

However, this model doesn't take into account the presence of the GTP cap, so Hinow et al[27]. extended the Dogterom-Liebler model in order to consider this part and develop a system of PDE describing the processes of growth, shortening, rescue, catastrophe and nucleation for MT polymerization, taking both tubulin in polymer form and free form into account.
The following equations characterize the model and they are divided in a system of two PDEs expressing the dynamics of growing (u) MTs and shrinking (v) MTs, and two ordinary differential equation (ODEs) expressing the conversion between free GTP (p) and GDP (q) bound tubulin.

$$\frac{\partial u(x,y,t)}{\partial t} = -\alpha(p(t))\frac{\partial u(x,y,t)}{\partial x} - \gamma\frac{\partial u(x,y,t)}{\partial y} \tag{2.3}$$

$$\frac{\partial v(x,t)}{\partial t} - \delta\frac{\partial v(x,t)}{\partial x} = \begin{cases} -R(t)u(x,y,t) & \text{if R(t)} < 0, \\ -\lambda v(x,t) & \text{if R(t)} > 0 \end{cases} \tag{2.4}$$

$$\frac{dp(t)}{dt} = -\alpha(p(t))\int_0^\infty \int_0^x u(x,y,t)dydx + \kappa q - \mu p^n \tag{2.5}$$

$$\frac{dq(t)}{dt} = \delta \int_0^\infty v(x,t)dx - \kappa q \tag{2.6}$$

The equations (2.3) and (2.4) describe the dynamics of the growing and shortening populations of MTs, where u(x,y,t) is the density of growing MTs with total length x and GDP zone size y at time t, α is the growth rate, p(t) is the concentration of GTP bound tubulin and the third term in (2.3) represents the progression of the GDP zone at the hydrolysis rate γ.

Moreover, v(x,t) is the density of shortening MTs of length x at time t, when the MTs don't have the GTP cap, so the MT is consists of GDP-tubulin. The second term describes MT shortening at a rate δ and the last term depends on the sign of R(t), which represent the progression rate of the GTP zone and is equal to αp(t) - γ. This last term represents the difference between the MT growth and hydrolysis rate. When $R(t) < 0$, hydrolysis happens faster than MT polymerization, so the MTs losing their GTP cap will shorten. While, when $R(t) \geq 0$ then the system is in a growing state and shortening MTs can be rescued with a rescue frequency, λ.

The ODEs (2.5) and (2.6) describe the evolution in time of the free GTP and GDP tubulin concentrations. The second and last terms of (2.5) represents the loss of GTP-tubulin as a result of uptake due to polymerization and nucleation,while the third term express the exchange between GTP and GDP. When MTs shorten at a rate δ, the concentration of free GDP tubulin increases and this what the second term in (2.6) represents.

In this model, however, there isn't a description for catastrophe frequency, despite the fact that growth and shortening rates, alongside rescue frequency, were model inputs.

An example of a more computational and quantitative mathematical model for MT

polymerization kinetics is the work by Marx and Mandelkow in 1994[32], based on the reaction cycle described by Mandelkow et al. (1988)[33] and on the assumption that the catastrophe rate depends only on the current state of the system or the work by Bolterauer et. al[34], where they develop a model in order to discuss specific assumptions that need to be implemented to obtain an adequate theoretical framework.

Chapter 3

Brain by the numbers

3.1 Neurons, neurodegeneration and neuronal loss in healthy and AD brain

At the question about what the precise number of neurons in the brain may be, many articles affirmed that the human brain presented about 100 billions neurons and 10 times more glial cells, but these affirmations usually didn't cite any references.

The reason for this, according to Suzana Herculano-Houzel's article[35], is that there was not an actual estimate of the number of neurons in the brain until 2009 by Azevedo et *al.*[36], who reported an estimation of about **86 billions** of neurons in the human brain.

At this day, the impact that neuronal loss has on information processing is still not clear, but it is estimated that in healthy brain approximately 85,000 neurons die every day, number that, in case of neurodegenerative diseases or brain injury, increases considerably[37].

The study carried on by Wegiel J. et *al* [38] provides a large and useful amount of information about brain structure- and stage of AD-specific dynamics of neuronal loss.

From a more general perspective, the study showed that the stage of mild cognitive impairment (MCI) and mild AD, indicated as **FAST 3-4**, of the duration of about 9 years is the stage with the largest percentage of neuronal loss, followed by an acceleration of neuronal loss and degeneration, reaching a ceiling level during the stage of moderate and moderately severe AD or **FAST 5-6**.

This stage has an average duration of 4 years, after which the stage of severe AD, or **FAST 7**, is reached. Here, the results suggest a decline of neuronal loss to a floor level.

Moreover, the estimations of neuronal loss don't concern only the stage of the disease, but also the different subdivisions in the brain: Entorhinal c. (all layers)(EC), Entorhinal c. (Islands)(EC-Is), CA1, CA2, CA3, CA4, subiculum (Sub), amygdala (Am), thalamus (Th), substantia nigra (SN), magnocellular basal complex (MBC) and dentate nucleus (DN).

In terms of percentage (**Fig.** 3.1), the average neuronal loss in MCI/moderate AD (FAST 3-4) is at 31%, which is almost twice the percentages in moderate/-moderately severe AD (FAST 5-6) and severe AD (FAST 7), 15.5% and 13.8% respectively. Besides, the differences between percentages of different subdivisions in the same stage reflect a structure-specific pattern of neuronal loss. The rate of neuronal loss in relation to the stage of the disease, is calculated per million neurons and is an index independent of the number of neurons in an individual brain structure.

In FAST 3-4 (**Fig.** 3.2), the average rate is 159 neuron loss/million/day, while in FAST 5-6 the value is 332 neuron loss/million/day, but is worth to notice that, in this stage, subdivisions show different behaviour between one another as some undergo a significant reduction of neuronal loss, while others a significant acceleration.

FAST 7, compared to the other stages, showed an important reduction of neuronal

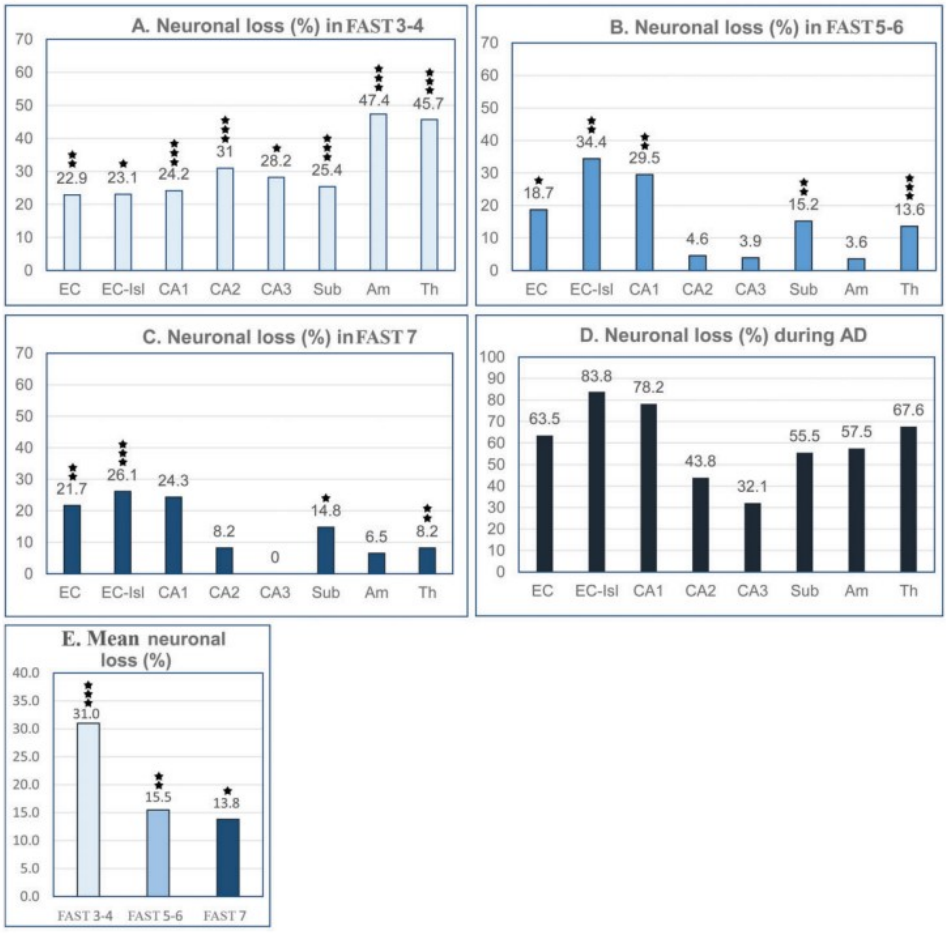

Figure 3.1: Graphs A–C show the percentage of neuronal loss for each subdivision in FAST 3-4, FAST 5-6 and FAST 7. **Graph D** shows cumulative neuronal loss percentage during the entire course of the disease. **Graph E** report the average percentage of neuronal loss in the three stages.[38]

loss, which at first glance might be unexpected and surprising, but in reality is a reflection of terminal exhaustion of the neuronal pool.

More in-depth, among the 12 subdivisions examined, 11 of them presented neurofibrillary tangles, with a percentage increasing with the progression of the disease, but in a structure-specific pattern.

In this thesis, the aim of the computational model is to simulate the rate of MTs

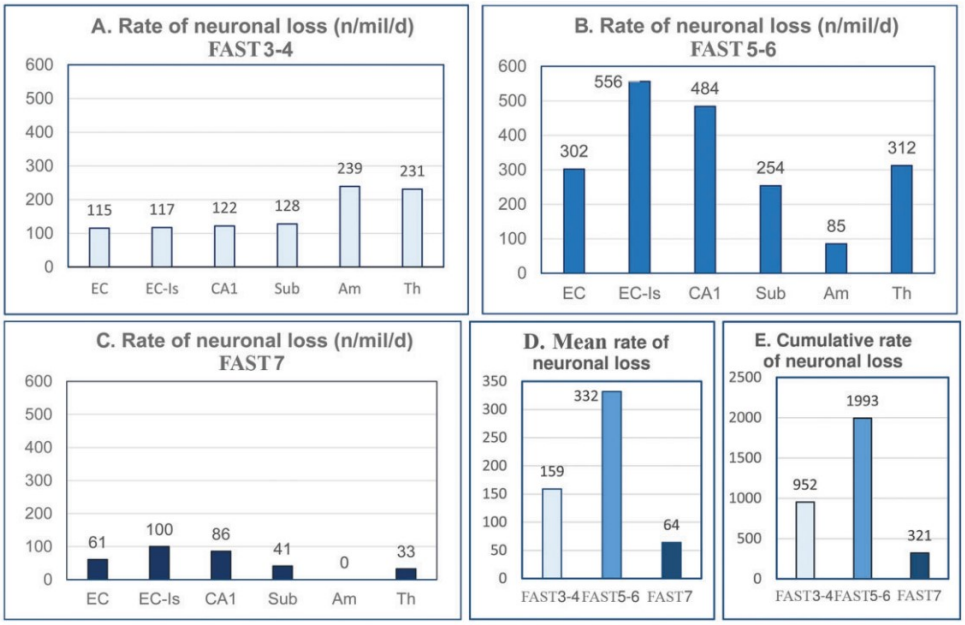

Figure 3.2: Graphs A–C Estimates of the rate of neuronal loss reveal strikingly different dynamics of neuronal loss in FAST stages 3–4, FAST stages 5–6, and FAST stage 7. **Graph D** shows the pattern of the rate of neuronal loss in terms of mean rate and **Graph E** in terms of cumulative neuronal loss.[38]

loss in neurons and predict the time needed for neurons to lose all MTs in function of hyperphosphorylated tau, and a first step in building this model is to get a clearer look of the neuronal loss rate, not only in measure of *neuron loss/million/day* but also in total neurons loss par day and par year (**Table** 3.1).

	Neuronal loss rate (/million/day)	**Neuronal loss rate** (/day)	**Neuronal loss rate** (/year)
Healthy brain		$85 \cdot 10^3$	$31.03 \cdot 10^6$
MCI/mild AD	159	$13.67 \cdot 10^6$	$4.99 \cdot 10^9$
Moderate/moderately severe AD	332	$28.55 \cdot 10^6$	$1.04 \cdot 10^{10}$
Severe AD	64	$5.50 \cdot 10^6$	$2.01 \cdot 10^9$

Table 3.1: Neuronal loss rate.

3.2 MTs and tubulin dimers: numbers and rate loss

A second step in building the computational model is to estimate the number of MTs and consequently of tubulin dimers, both in a neuron and in the brain, and then calculate their rate loss based on the values in Table 3.1.

The average volume of a neuron is set to be approximately 1041 μm^3 [39], while the volume of a microtubule with a diameter of 25 nm and 20 μm long is about $9.81 \cdot 10^{-3}$ μm^3, so comparing the volumes, it can be estimated that in a neuron there are approximately 106000 MTs. Considering the whole brain, this number increases to $9.12 \cdot 10^{15}$.

As previously mentioned, a MT consists in 13 protofilaments of tubulin dimers 8 nm long and, in a 20 μm MT, the total number of tubulin dimers can be calculated as the product of 13x20x1250, so a total of 325000 tubulin dimers in a microtubule. This estimation referred to the brain would be $2.96 \cdot 10^{21}$.

	Number (/neuron)	**Number** (/brain)
Neurons		$86 \cdot 10^9$
MTs	$1.06 \cdot 10^5$	$9.12 \cdot 10^{15}$
Tubulin dimers	$3.25 \cdot 10^5$	$2.96 \cdot 10^{21}$

Table 3.2: Summary of the numbers of neurons, MTs and tubulin dimers.

Knowing these values, it is possible to calculate the loss rate of MTs and tubulin dimers, both in healthy and AD brain.

		Healthy brain	MCI/mild AD	Moderate/moderately severe AD	Severe AD
Neurons	/day	$85 \cdot 10^3$	$13.67 \cdot 10^6$	$28.55 \cdot 10^6$	$5.50 \cdot 10^6$
	/year	$3.10 \cdot 10^7$	$4.99 \cdot 10^9$	$1.04 \cdot 10^{10}$	$2.01 \cdot 10^9$
MTs	/day	$9.01 \cdot 10^9$	$1.45 \cdot 10^{12}$	$3.03 \cdot 10^{12}$	$5.83 \cdot 10^{11}$
	/year	$3.29 \cdot 10^{12}$	$5.29 \cdot 10^{14}$	$1.11 \cdot 10^{15}$	$2.13 \cdot 10^{14}$
Tubulin dimers	/day	$2.93 \cdot 10^{15}$	$4.71 \cdot 10^{17}$	$9.85 \cdot 10^{17}$	$1.89 \cdot 10^{17}$
	/year	$1.07 \cdot 10^{18}$	$1.72 \cdot 10^{20}$	$3.60 \cdot 10^{20}$	$6.90 \cdot 10^{19}$

Table 3.3: Rate loss of neurons, MTs and tubulin dimers measured par day and par year. The values are all referred to the brain.

3.3 Tau and MTs

As already mentioned, tau protein and MTs are strongly correlated as their bond increase the rate of assembly and stability of MTs. In pathological conditions, tau reaches an hyperphosphorylated state, thus the strength of this bond decreases.
To get an idea of how this bond changes from a quantitative point of view, the values of free-binding energy between tau and MTs, in normal conditions and when all Serines residues resulted phosphorylated, were confronted.
The rate constant can be expressed through the Arrhenius equation:

$$k_d = Ae^{\frac{-\Delta G^0}{RT}}$$

where A is a constant for the frequency of particle collisions, ΔG^0 is Gibbs free-binding energy, R is the universal gas constant, and T is the temperature expressed in Kelvin. From this equation, it is evident that temperature is a significant factor that affects the rate of a chemical reaction.
In this case, the values considered were calculated by Luca Congiu with Molecular Operating Environment (MOE) software and reported in his Master's degree thesis "Computational investigations of the link between hyperphosphorylation of MAP tau and melatonin binding in Alzheimer's disease"[40]. These values correspond to the free-binding energy of tau and MTs in normal conditions at 37° and the contribution of each serine.

The free-binding energy of tau and tubulin in pathological conditions was estimated subtracting from the value in normal conditions the serine residues contribution and from the result obtained the rate constant k_d was deducted. Comparing these numbers, it is possible to notice how in AD, the affinity costant value between tau and MTs is significantly increased, meaning that the binding and the affinity are considerably weaker.

	Value
Tau-MT	-197.7 ± 44
SER208	-1.1 ± 3
SER210	0.7 ± 1.5
SER214	-2.7 ± 2.4
SER235	-2.1 ± 3.3
SER237	-2.8 ± 3.4
SER238	-0.8 ± 4.9
SER241	-4.5 ± 1.8
SER258	-10.3 ± 3.9
SER262	-6.1 ± 5.5
SER285	-2.4 ± 4.6
SER289	-13.2 ± 2.9
SER293	-6.8 ± 6.6
SER305	-4 ± 4.3
SER316	-2 ± 3.3
SER320	-9.4 ± 6
SER324	-5.1 ± 3.3
SER341	-0.18 ± 0.6
SER352	-0.5 ± 0.1
SER356	-0.7 ± 0.2

Table 3.4: Free-binding energy [kJ/mol], Tau-Microtubules.

	ΔG^0	k_d
Healthy brain	-197.7 ± 44	$4.34 \cdot 10^{-34}$
AD brain	-123.72 ± 105.5	$1.43 \cdot 10^{-21}$

Table 3.5: Free-binding energy [kJ/mol] and rate constant, Tau-Microtubules.

Another information regarding tau and MTs worth considering is that when tau binds to MTs, it reaches saturation at a molar ratio of 1 tau per ∼5–10 tubulin dimers, meaning there are several binding sites along the length of an MT[41].

Chapter 4

Computational model

4.1 Model description

As mentioned in chapter 2, there are several computational and theoretical models that describe MTs dynamics. At first, a kinetic model, described in **Appendix A**, was developed focusing more on phosphorylation dynamics and on evaluating the effect of different kinases and phosphatases. It included a more complete set of equations, but the lack of parameter values did not make possibile its use.
As a result, the model this thesis refers to and use as a basis is the one published by Dogterom and Leibler in 1993[31], a simplistic model that delineates growing and shortening length distributions of MTs through a partial differential equation (PDE) system. The starting equations, focused on the time-dependent probability densities of growing MTs, u and shrinking MTs, v are:

$$\frac{\partial u(x,t)}{\partial t} = -f_c u(x,t) + f_r v(x,t) - v_g \frac{\partial u(x,t)}{\partial x} \tag{4.1}$$

$$\frac{\partial v(x,t)}{\partial t} = f_c u(x,t) - f_r v(x,t) + v_s \frac{\partial v(x,t)}{\partial x} \tag{4.2}$$

To calculate the solutions from (4.1) and (4.2), some assumptions have been made. One of these, is that asymptotically $\frac{du}{dt} = \frac{dv}{dt} = 0$, obtaining this way the system

$$0 = -f_c u(x) + f_r v(x) - v_g \frac{du}{dx} \tag{4.3}$$

$$0 = f_c u(x) - f_r v(x) + v_s \frac{dv}{dx} \tag{4.4}$$

from which the stationary solutions u(x) and v(x) have been determined

$$u(x) = C_3 \exp \frac{-f_c x}{v_g} + \exp \frac{-f_c x}{v_g} \Big(\frac{C_1 f_r \exp \frac{-f_c x}{v_g}}{f_c} \Big) + \frac{C_2 v_s \exp \frac{f_r x}{v_s}}{v_g} \tag{4.5}$$

$$v(x) = C_1 + C_2 \exp \frac{-x(f_c v_s - f_r v_g)}{v_g v_s} \tag{4.6}$$

with C_1, C_2 and C_3 constants. To determined these, initial conditions are needed, so for x = 0, the functions u(x) and v(x) are considered equal to the half of the total MTs in the brain, while the first derivative of v(x) for x = 0 equals 0.

$$\begin{aligned} v(0) &= 4.56 \cdot 10^{15} \\ v'(0) &= 0 \\ u(0) &= 4.56 \cdot 10^{15} \end{aligned} \tag{4.7}$$

After obtaining the constants C_1, C_2 and C_3, the solutions u(x) and v(x) can be rewritten. As for the parameters describing dynamic instability f_c, v_g and v_s, three cases have been distinguished:

1. Only tubulin at 3 μM, considered as the control case
2. Tubulin at 3 μM and native tau at 0.5 μM
3. Tubulin at 3 μM and phosphorylated tau at 0.5 μM.

The values for each case are the one published by D.N. Drechsel et al. in 1992[42].

	$v_g(\frac{\mu m}{min})$	$f_c(\frac{1}{min})$	$v_s(\frac{\mu m}{min})$
Tubulin alone	0.38	0.54	10.8
Tubulin - native tau	0.97	0	5.28
Tubulin - phosphorylated tau	0.34	0.036	10.8*

Table 4.1: Values for f_c, v_g and v_s. * the value was not published, so as reference it was chosen the same value for tubulin alone.

About the rescue frequency f_r, it has been scaled to be between 0 and 1 and its value is considered proportional to the rate of tau phosphorylation. Specifically, if $f_r = 0$, this would mean that all of tau concentration has been phosphorylated, so the MTs are no longer stable, while if $f_r = 1$, tau is not phosphorylated, so it's still bound to the MTs, stabilizing them. In order to have a better view of how f_r influences u(x), the values between 0 and 1 have been changed with a step of 0.05.

With all four parameters, u(x) and v(x) can be calculated and, consequently, plotted in order to have a graphical visualization of the functions.
Then, the following step consists in the estimation of the mean length in the growing phase, $\overline{x_g}$, and in the shrinking phase, $\overline{x_s}$. There parameters are calculated as the indefinite integral of the product between x and the probability density function, divided then by the indefinite integral of the probability density considered.

$$\overline{x_g}(x) = \frac{\int x \cdot u(x)dx}{\int u(x)dx} \tag{4.8}$$

$$\overline{x_s}(x) = \frac{\int x \cdot v(x)dx}{\int v(x)dx} \tag{4.9}$$

After calculating (4.8) and (4.9), they can also be plotted in order to see, how in both phases, the mean length can change depending on the input length of the MTs. In the end, to get a general prospective of both u(x) and v(x), their differences is calculated and then plotted, in order to understand the net effect in each case and evaluate if there are correspondences with experimental data of the pathology.

Chapter 5

Results and discussion

5.1 Model results

As mentioned in the previous chapter, equations (4.5) and (4.6) are respectively the probability density of growing and shrinking MTs, and, depending on the parameters defining dynamic instability, these functions change their expression. More in depth, with the initial conditions considered for solving the differential equations (4.3) and (4.4), it can be observed that the probability density u(x) changes in each case considered and for every rescue frequency considered and, consequently, also the expression of $\overline{x_g}(x)$ changes at the changing of the parameters, while the probability density v(x) remains constant at the initial value of half of the MTs in the brain in each case, meaning also that $\overline{x_s}(x)$ always corresponds to a linear function.

5.1.1 Control case: tubulin alone

In **Fig.** 5.1 it can be observed how the frequency of rescue influences u(x). For f_r between 0.55 and 1, the probability density increase for x between 0 and 5 μm reaching a peak value, after which the evolution remains stable. Moreover, the initial increase is more rapid at higher frequencies. On the other hand, for f_r

between 0 and 0.50, the situation is reversed, so for x between 0 and 5 μm, u(x) decrease to a minimum value before levelling out.
This means that, for short lengths of MTs, the probability density of growing MTs changes significantly, while for longer MTs, u(x) shows a steady trend.

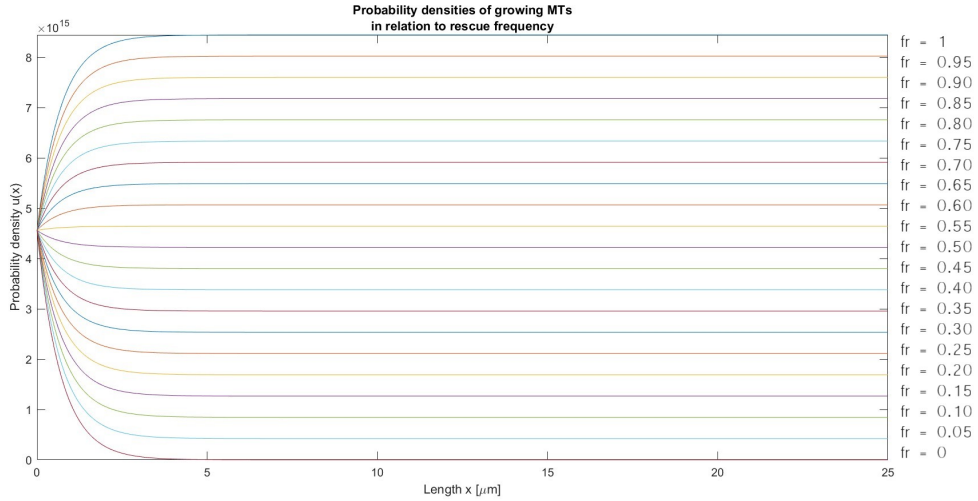

Figure 5.1: Probability density of growing MTs u(x) at different values of rescue frequency.

Fig 5.2 shows, instead, the evolution of the mean length of MTs in relation to the maximum length x for the same rescue frequencies of **Fig.** 5.1.

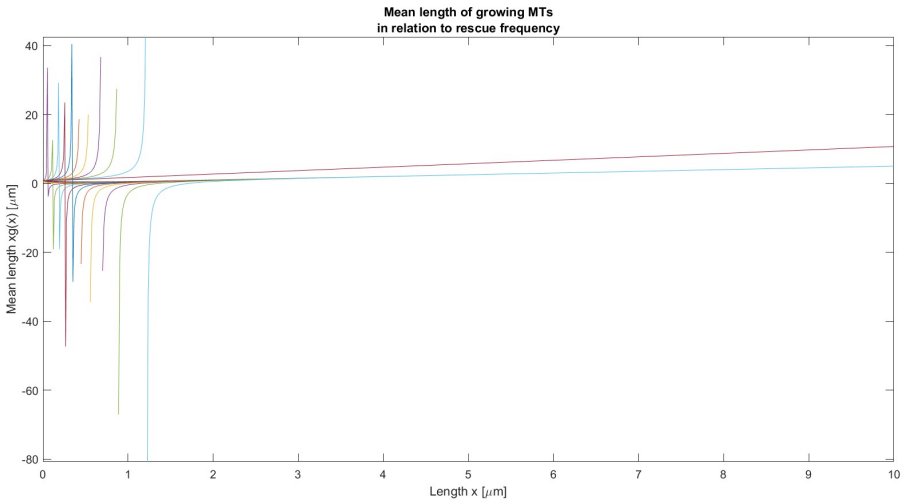

Figure 5.2: Mean length $\overline{x_g}(x)$ at different values of rescue frequency. Each color correspond to the same f_r in Fig 5.1.

In this case, three different behaviours can be distinguished:

1. for f_r between 0.55 and 1, $\overline{x_g}(x)$ (**Fig.** 5.3) shows a decrease to a minimum value, followed by a rapid and linear increase, meaning that for shorter MTs, rescue frequencies have a higher effect towards MTs in comparison to longer MTs, for which the average length seems to increase linearly.

   For this reason, linear regression has been done and the linear equations collected (**Table** 5.1) for each f_r showed a minimal difference, highlighting the fact that, for MTs longer than $\sim$3 μm, the rescue frequency doesn't influence the average length of the microtubules.

   Moreover, **Table** 5.1 shows that the angular coefficients are approximately 0.5, so for every maximum length x, the average one would be half the value, indicating the presence of MTs population of different lengths. Considering the pathology of AD, this behaviour could be interpreted as a possibility to overcome the reduction of f_r due to tau hyperphosphorylation if MTs can be

stabilized by an external agents, allowing them to grow longer.

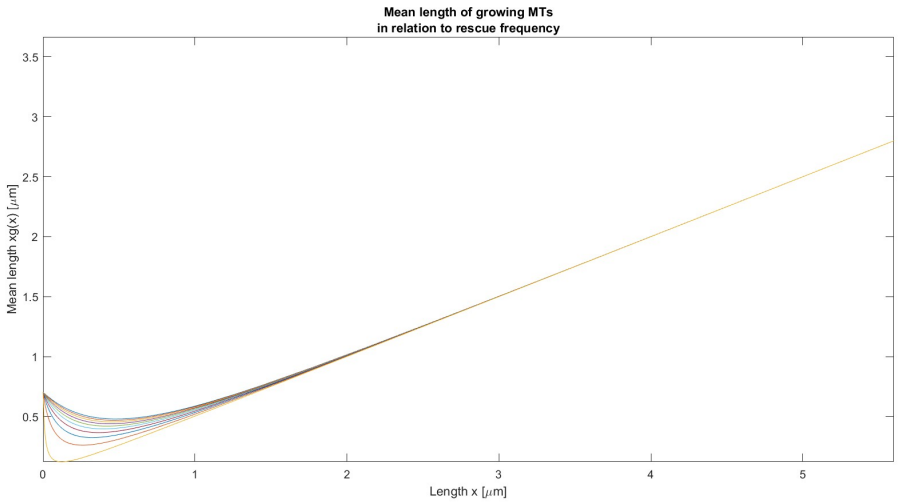

Figure 5.3: Mean length $\overline{x_g}(x)$ for values of rescue frequency between 0.55 and 1.

f_r	**Linear equation**
0.55	y = 0.494x + 0.103
0.60	y = 0.494x + 0.106
0.65	y = 0.494x + 0.108
0.70	y = 0.494x + 0.110
0.75	y = 0.494x + 0.111
0.80	y = 0.493x + 0.113
0.85	y = 0.493x + 0.114
0.90	y = 0.493x + 0.115
0.95	y = 0.493x + 0.116
1	y = 0.493x + 0.118

Table 5.1: Linear equations calculated from linear regression.

2. for f_r between 0.05 and 0.45, a much different behaviour of $\overline{x_g}(x)$ can be observed (**Fig.** 5.4). There is a substantial increase for small changes of x, reaching peak levels of mean length, followed by a sudden collapse, as biologically and physically a length can't assume a negative value. The high values of $\overline{x_g}(x)$ can be biologically justified considering that MTs are generally 200 nm to 25 μm long, but in axons their length may reach 50 - 100 μm[43].

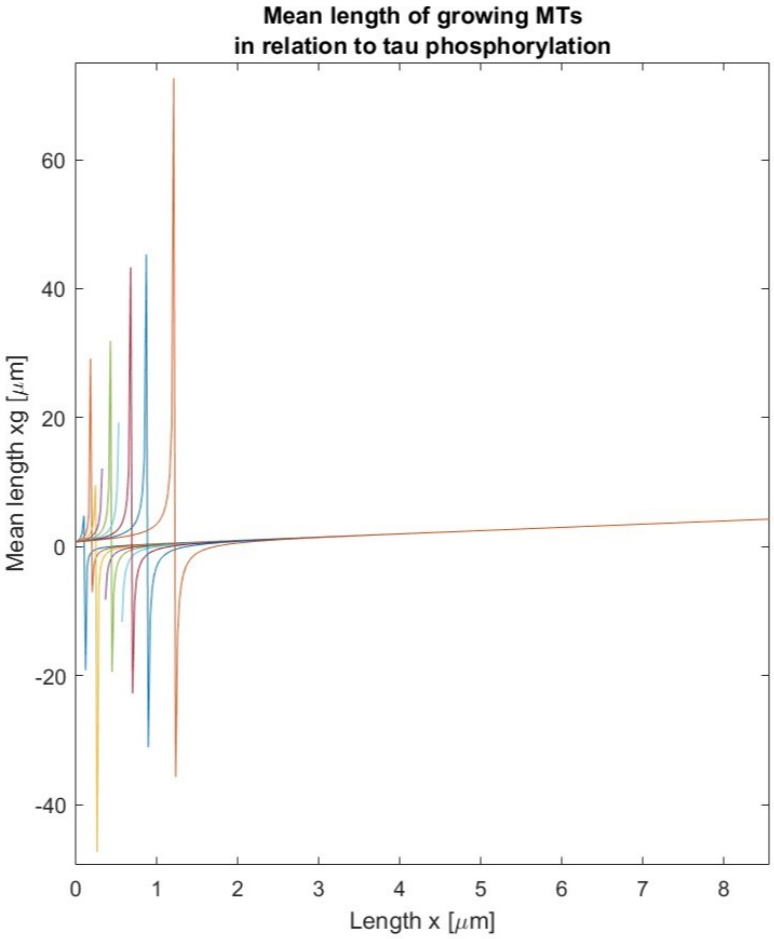

Figure 5.4: Mean length $\overline{x_g}(x)$ for values of rescue frequency between 0.05 and 0.45.

3. for $f_r = 0$, $\overline{x_g}(x)$ is a linear function (**Fig.** 5.5), so the average length of growing MTs increases linearly at the increase of maximum length x, with an angular coefficient a little above 1, so for a certain maximum length x, the average is slightly longer, indicating a population of MTs with different, but also similar lengths.

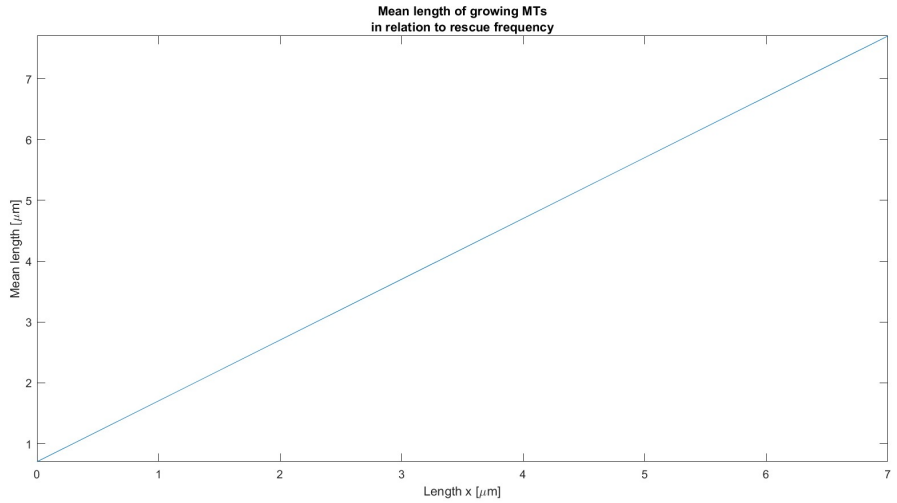

Figure 5.5: Mean length $\overline{x_g}(x)$ for $f_r = 0$

As mentioned before, the probability density of shrinking MTs v(x), given the first derivative initial condition (4.7), results in a constant value equal to half of the MTs number in the brain, meaning that for any given length the shrinking phase of MTs doesn't undergo any changes, but remains the same (**Fig.** 5.6). In **Fig.** 5.7, the average length of shrinking MTs $\overline{x_s}(x)$ shows an increasing linear trend, with an angular coefficient of approximately 0.5, so as mentioned before, it indicates a MTs population with different lengths.

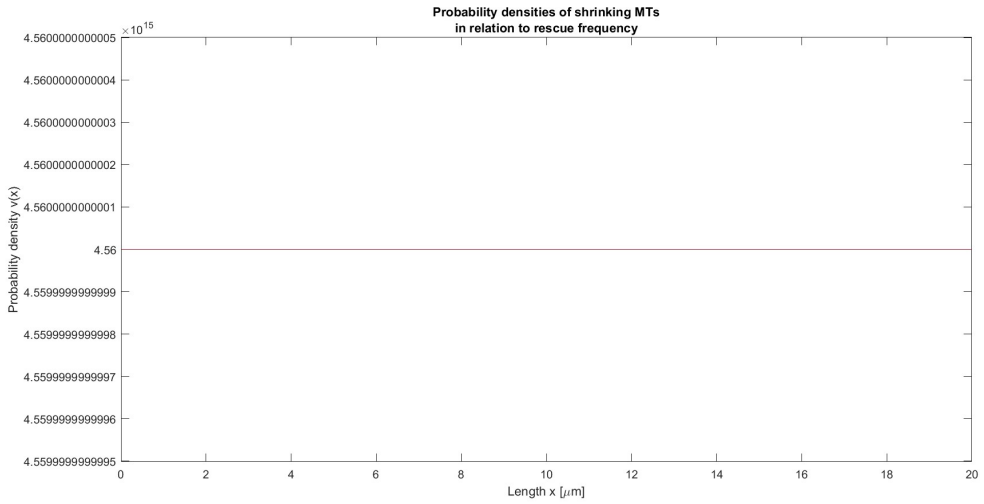

Figure 5.6: Probability density of shrinking MTs v(x).

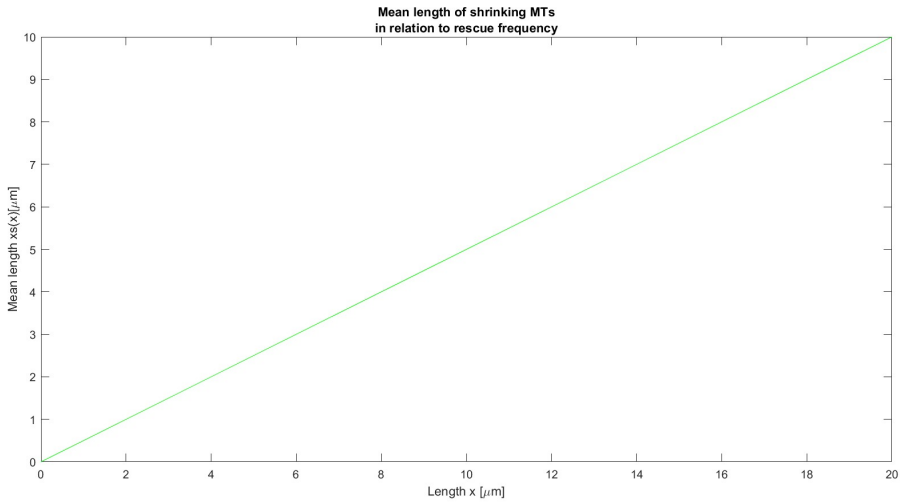

Figure 5.7: Mean length $\overline{x_g}(x)$ at different values of rescue frequency. Each color correspond to the same f_r in Fig 5.1.

5.1.2 Tubulin and native tau

In this case, the probability density u(x) in relation to both tubulin and native tau has been analyzed. **Fig.** 5.8 shows a linear relation between x and u (x), corresponding to a linear growth that can be up to 10-fold greater than the initial value, as f_r increases.

Considering that in this case f_c is 0, this means that microtubules wouldn't undergo catastrophe, justifying this way the monotonic linear growth, and as f_r increases, the quantity of tau protein bound to MTs is higher, promoting so their stabilization.

Pathologically speaking, **Fig.** 5.8 may represent the transition from an healthy brain, given by u(x) for higher rescue frequencies, to the early stages of AD as f_r decreases due to the subtraction of tau from MTs consequent to its phosphorylation, limiting so the possibility of growth for MTs.

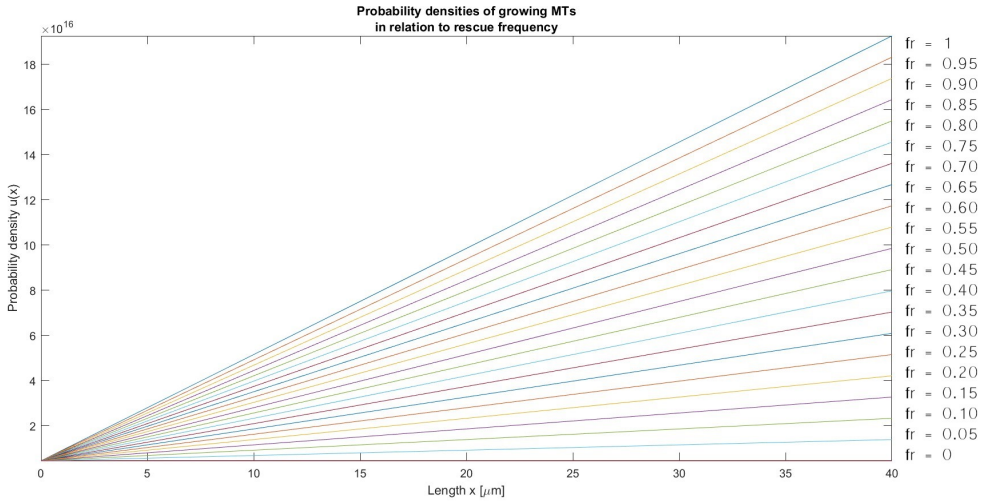

Figure 5.8: Probability density of growing MTs u(x) at different values of rescue frequency.

A similar linear trend can be observed in **Fig.** 5.9 showing the average length of growing MTs. The angular coefficients of these equations measure around ∼0.5, so as length x increases, $\overline{x_g}(x)$ measures approximately half, and as already mentioned above, this highlights a population of MTs with different lengths.
Moreover, as said for u(x), an f_r decrease translates in a slower rise of the average length, indicating that a smaller quantity of tau bound to MTs leads to a limited growth, sign of beginning stages of AD.

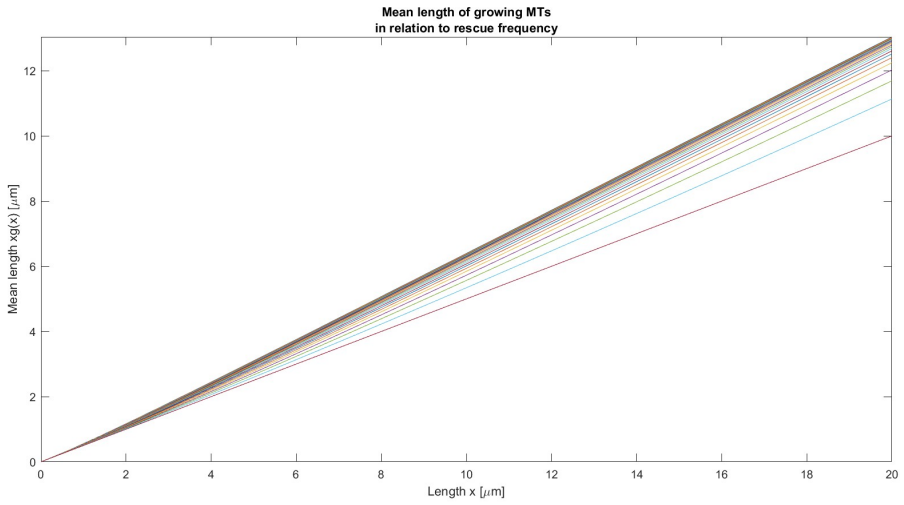

Figure 5.9: Mean length $\overline{x_g}(x)$ at different values of rescue frequency. Each color correspond to the same f_r in Fig 5.8.

As for the probability density of shrinking MTs v(x) and their mean length $\overline{x_s}(x)$, there aren't variations from **Fig.** 5.6 and **Fig.** 5.7, so v(x) remains constant, while $\overline{x_s}(x)$ maintains its linear trend, meaning that the considerations are still valid.

5.1.3 Tubulin and phosphorylated tau

In **Fig.** 5.10, the probability density of growing MTs u(x) for $f_r = 0$ shows a decreasing trend before levelling out to a floor level, while for higher rescue frequencies u(x) shows a significant and rapid increase that can be up to 10-fold or more of the initial value.

These may represent the moderate and late stage of AD, especially the lower rescue frequencies, when the quantity of phosphorylated tau increases at the expense of the tau bound to MTs, slowing the growth of MTs to a steady level or, as for $f_r = 0$, decreasing the probability of growth for microtubules. One thing in common between all f_r, is that for maximum lenght x > ∼70 μm, the probability density of growing MTs remains steady.

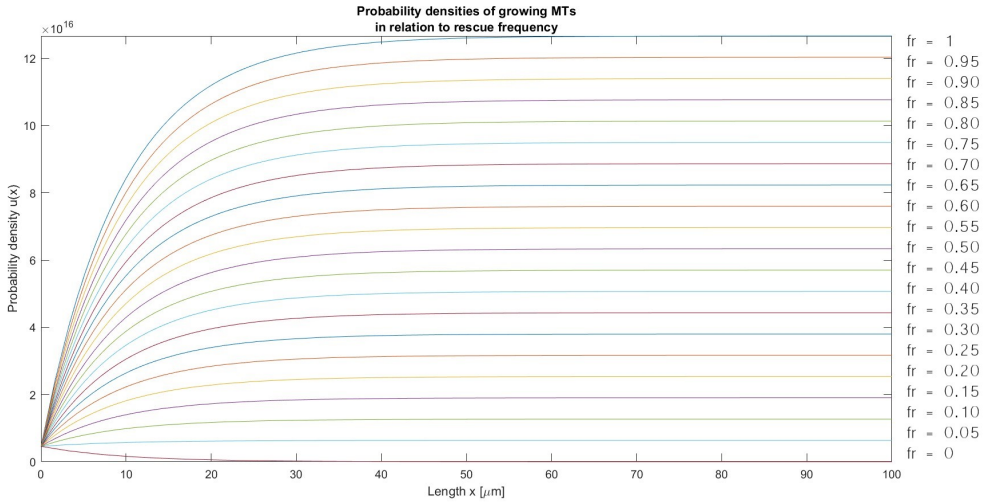

Figure 5.10: Probability density of growing MTs u(x) at different values of rescue frequency.

About the mean length of growing MTs for $f_r = 0$, $\overline{x_g}(x)$ is a linear function, but for the other rescue frequencies, it can be observed a slow decrease to a minimum value, followed by gradual rise (**Fig.** 5.11). This behaviour is similar to the one represented in **Fig.** 5.3, so the possibility to overcome the reduction of f_r due to tau hyperphosphorylation with the help of external agents in order to stabilize microtubules may be valid also in this case.

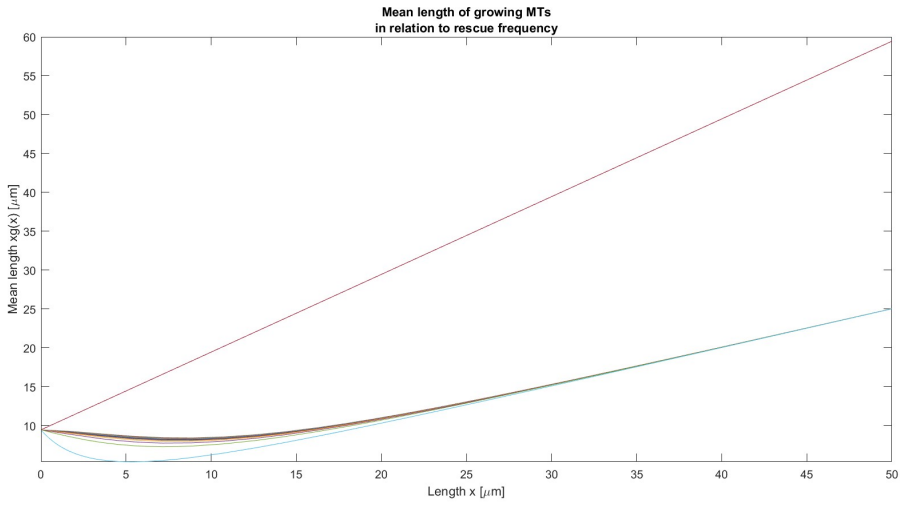

Figure 5.11: Mean length $\overline{x_g}(x)$ at different values of rescue frequency. Each color correspond to the same f_r in Fig 5.10.

As for the considered case with tubulin alone and with tubulin and native tau, v(x) and $\overline{x_s}(x)$ are still represented by **Fig.** 5.6 and **Fig.** 5.7, respectively.

5.1.4 Balance of growth and shrinking MTs

In the previous sections, the probability density of growing and shrinking MTs have been analyzed separately and in different conditions, but in order to have an idea of what happens in the brain they have to be studied together.
In an healthy brain, the phases of growth and shrinkage of microtubules, where MTs are able to grow and break, but also be rescued so they can regrow again, alternate in a continuous way.
Moreover, if the difference between u(x) and v(x) would be investigated, the net effect in this case would be almost a balance, but in pathological conditions this balanced situation is not achievable, as the MTs instability increase, leading to a rise of shrinkage rate without possibility of rescue.
Considering the case of tubulin alone, it is possible to see that for higher rescue frequencies, the probability density is considerably reduced, but yet positive, meaning that MTs continue growing (**Fig.** 5.12). On the other hand, for lower rescue frequencies, the difference leads to a negative balance where the shrinking MTs exceed the growing ones.

As for the tubulin and tau case, the difference is almost imperceptible, but graphically it can be seen in the traslation for x = 0, in **Fig.** 5.8 u(0) = $4.56 \cdot 10^{15}$, while in this case for x = 0, u(x) - v(x) = 0.
This indicates that, except for f_r where the function is 0, for all the other rescue frequencies MTs are able to keep growing. From a pathological point of view, **Fig.** 5.13 may represent the evolution from an healthy state to early signs of the pathology as the rescue frequencies decrease.

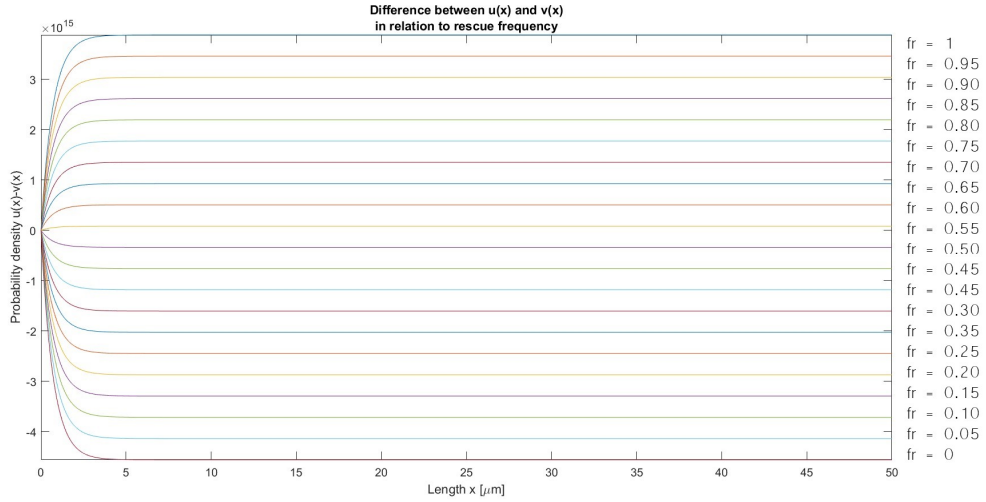

Figure 5.12: Difference between probability density of growing MTs and shrinking MTs, for different values of f_r in case of only tubulin.

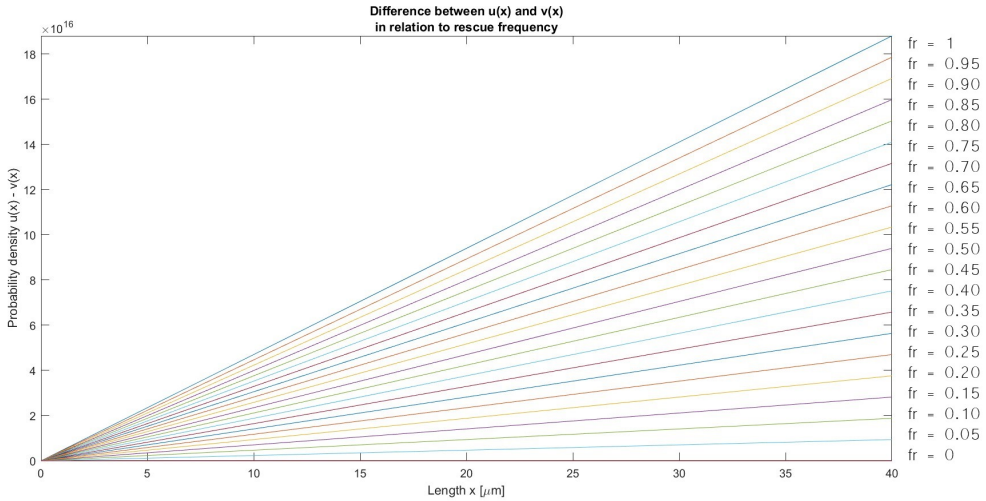

Figure 5.13: Difference between probability density of growing MTs and shrinking MTs, for different values of f_r, considering tubulin and native tau.

Considering tubulin and phosphorylated tau, the difference may be observed, as in for tubulin and native tau, in the traslation of the functions (**Fig.** 5.14).
For higher f_r, MTs are still able to grow, but for lower frequencies, growth is very limited, until v(x) exceeds u(x) reaching a negative balance.
This behaviour could represent the moderate and moderately severe stages of AD, when the yearly rate loss of MTs reaches an order of magnitude of 16.

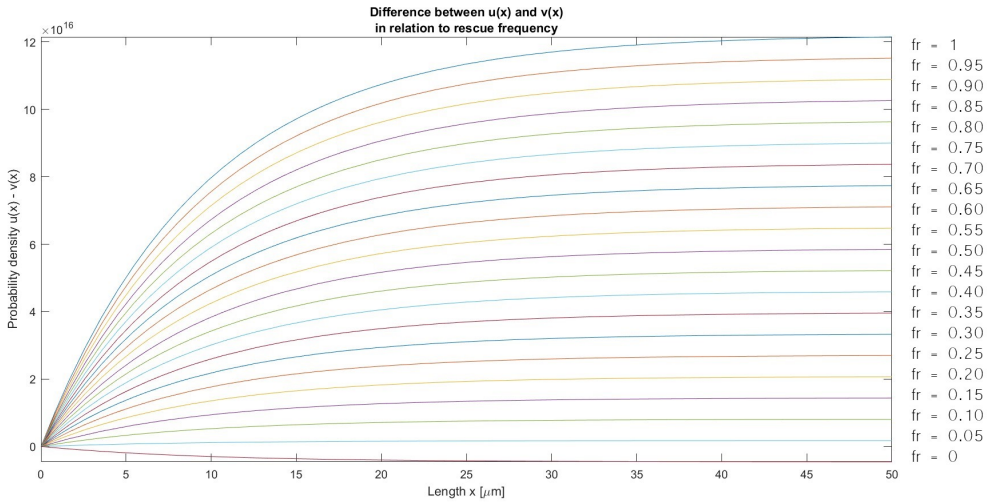

Figure 5.14: Difference between probability density of growing MTs and shrinking MTs, for different values of f_r, considering tubulin and phosphorylated tau.

Chapter 6

Conclusion

AD is the most common form of dementia according to studies, and for years researchers have focused on exploring hypothesis on possible causes of the disease. Two of these hypothesis are the ones on which studies focus the most, and they regard β-amyloid and tau protein. The first one has been extensively studied, but recent research uncovered some data falsification in the first works, questioning so the validation of this theory.

Following this, the tau hypothesis gained even more attention than it already had and, for this reason, tau protein was and still is the target of many therapeutic studies.

The goal of this work is to develop a computation model describing the cellular mechanism of Alzheimer's disease initiation due to tau protein hyperphosphorylation. To do this, several models have been explored and studied, and the one taken as a reference was the Dogterom-Leibler's model which focuses on the phases of growth and shrinkage of MTs dynamics instability in relation to time and MTs' length.

With appropriate considerations and approximations, the developed model describes the probability density of growing and shrinking MTs and also the average length of MTs in stationary conditions, and in relation not only on MTs' length, but

also on rescue frequency, which in turn depends on tau state of phosphorylation. With the results obtained, it can be seen that this model manages to reflect the passage from an healthy state of the brain to the early stages of AD when tubulin and native tau are considered, specifically for high rescue frequencies, showing a linear and consistent growth of MTs, and also manages to represent the moderate and moderately severe stages of AD when tubulin and phosphorylated tau are considered for lower rescue frequencies.

But what is most important is that the model shows how the increase of the rescue frequency, obtainable by inhibiting tau phosphorylation perhaps with external pharmacological agents, would allow MTs to be rescued and, consequently, regrow meaning that inhibiting tau phosphorylation would slow down the progress of the disease.

It's worth underlining that this model is a simplistic one, but it can be a starting point for future studies where the solutions may be time-dependent or the PDE system may include more equations to describe in more detail dynamic instability or also a tau phosphorylation inhibitor can be considered, the possibilities are many.

Appendix A

Kinetic model

As mentioned in Chapter 4, before starting working with the Dogterom-Leibler model, several others have been developed and explored.
The first one developed consisted in a set of equations, both integral and differential, describing:

1. tau phosphorylation by GSK3β, CaMKII and CDK1
2. MTs phosphorylation by GSK3β, CaMKII and CDK1
3. tau dephosphorylation by PP2A
4. MTs dephosphorylation by PP2A
5. NFTs formation
6. MTs polymerization and depolymerization.

The kinetics of a reaction is described through mathematical relationships that connect the rate of the reaction itself to the concentration of the species present ([A] and [B]) through parameters set by thermodynamics called rate constants (k). The terms (a, b) are exponents of the concentrations and represent the reaction

orders which often differ from the stoichiometric coefficients of the reaction.

$$\mathrm{a[A] + b[B] \xrightarrow{k} [P]}$$

The rate of the equation can be calculated as:

$$Rate = k[A]^a[B]^b$$

or be expressed through the Arrhenius equation:

$$k = Ae^{\frac{-E_a}{RT}}$$

The differential form of rate law usually is used to describe the processes occurring on a molecular level during a reaction, whereas the integrated one is used for determining the reaction order and the value of the rate constant from experimental measurements.
The first-order chemical reaction can be written as:

$$\mathrm{[A] \xrightarrow{k} [P]}$$

And the differential equation describing the kinetics of this reaction is:

$$Rate = -\frac{d[A]}{dt} = k[A]$$

The reaction rate is measured in mol/s and the kinetic constant in 1/s, however the unit of measure of the reaction rate constant differs depending on the order of the equation.
Upon integration, the equation can be written as:

$$\ln[A] = -kt + \ln[A(0)]$$

or

$$[A] = [A(0)]e^{-kt}$$

where [A(0)] indicates the reactant concentration at t=0.
In case the sum of the exponents in the rate law equals two, and differently form the first-order equation, the unit of measure of the reaction rate is $M^{-1}s^{-1}$. Furthermore, there is also a classification of these equation depending on the reactants involved, specifically if they are identical or different. In the first case, the corresponding reaction would be:

$$2\,[\mathrm{A}] \xrightarrow{\mathrm{k}} [\mathrm{P}]$$

Resulting in the following differential equation

$$Rate = -\frac{d[A]}{dt} = k[A]^2$$

and integral form

$$\frac{1}{[A]} = \frac{1}{[A(0)]} + kt$$

If the case is that of multiple reactants, they are combining in a single step

$$[\mathrm{A}] + [\mathrm{B}] \xrightarrow{\mathrm{k}} [\mathrm{P}]$$

where the reaction rate can be written as

$$Rate = -\frac{d[A]}{dt} = k[A][B]$$

and the integral rate equation obtainable

$$\ln \frac{[B][A(0)]}{[B(0)][A]} = k([B(0)] - [A(0)])t$$

With these concepts, the chemical reactions and related kinetic equation for the model can be written. The symbol $*$ indicates the phosphorylated state of the element considered.

1. Tau phosphorylation by GSK3β, CaMKII and CDK1:

   $\text{tau} + \text{GSK3}\beta \xrightarrow{\text{k}_1} \text{tau}^*$

   $\text{tau} + \text{CaMKII} \xrightarrow{\text{k}_2} \text{tau}^*$

   $\text{tau} + \text{CDK1} \xrightarrow{\text{k}_3} \text{tau}^*$

Integral Form	**Differential Form**
$\ln \frac{[GSK3\beta][tau(0)]}{[GSK3\beta(0)][tau]} = k_1([GSK3\beta(0)] - [tau(0)])t$	$-\frac{d[tau]}{dt} = k_1[tau][GSK3\beta]$
$\ln \frac{[CaMKII][tau(0)]}{[CaMKII(0)][tau]} = k_2([CaMKII(0)] - [tau(0)])t$	$-\frac{d[tau]}{dt} = k_2[tau][CaMKII]$
$\ln \frac{[CDK1][tau(0)]}{[CDK1(0)][tau]} = k_3([CDK1(0)] - [tau(0)])t$	$-\frac{d[tau]}{dt} = k_3[tau][CDK1]$

Table A.1: First-order kinetic equations describing tau phosphorylation.

2. MTs phosphorylation by GSK3β, CaMKII and CDK1:

   $\text{MT} + \text{GSK3}\beta \xrightarrow{\text{k}_5} \text{MT}^*$

   $\text{MT} + \text{CaMKII} \xrightarrow{\text{k}_6} \text{MT}^*$

   $\text{MT} + \text{CDK1} \xrightarrow{\text{k}_7} \text{MT}^*$

Integral Form	Differential Form
$\ln \frac{[GSK3\beta][MT(0)]}{[GSK3\beta(0)][MT]} = k_5([GSK3\beta(0)] - [MT(0)])t$	$-\frac{d[MT]}{dt} = k_5[MT][GSK3\beta]$
$\ln \frac{[CaMKII][MT(0)]}{[CaMKII(0)][MT]} = k_6([CaMKII(0)] - [MT(0)])t$	$-\frac{d[MT]}{dt} = k_6[MT][CaMKII]$
$\ln \frac{[CDK1][MT(0)]}{[CDK1(0)][MT]} = k_7([CDK1(0)] - [MT(0)])t$	$-\frac{d[MT]}{dt} = k_7[MT][CDK1]$

Table A.2: First-order kinetic equations describing MTs phosphorylation.

3. tau dephosphorylation by PP2A:

   $\text{tau}^* + \text{PP2A} \xrightarrow{\text{k}_4} \text{tau}$

Integral Form	Differential Form
$\ln \frac{[PP2A][tau^*(0)]}{[PP2A(0)][tau^*]} = k_4([PP2A(0)] - [tau^*(0)])t$	$-\frac{d[tau^*]}{dt} = k_4[tau^*][PP2A]$

Table A.3: First-order kinetic equation describing tau dephosphorylation.

4. MTs dephosphorylation by PP2A:

   $\text{MT}^* + \text{PP2A} \xrightarrow{\text{k}_8} \text{MT}$

Integral Form	Differential Form
$\ln \frac{[PP2A][MT^*(0)]}{[PP2A(0)][MT^*]} = k_8([PP2A(0)] - [MT^*(0)])t$	$-\frac{d[MT^*]}{dt} = k_8[MT^*][PP2A]$

Table A.4: First-order kinetic equation describing MTs dephosphorylation.

5. NFTs formation:

   $\text{tau}^* + \text{tau}^* \xrightarrow{\text{k}_{\text{NFT}}} \text{Ftau}$

Integral Form	Differential Form
$\frac{1}{[tau^*]} = \frac{1}{[tau^*(0)]} + k_{NFT}t$	$-\frac{d[tau^*]}{dt} = k_{NFT}[tau^*]^2$

Table A.5: Second-order kinetic equation describing NFTs formation.

6. MTs polymerization and depolymerization:

   $\text{Tu} \underset{\overline{k}_d}{\overset{k_p}{\rightleftharpoons}} \text{MT}$

   with $\overline{k}_d$=k_d + k_t[tau(t)], as the depolymerization of microtubules depends on the concentration of phosphorylated tau.

Integral Form	Differential Form
$\ln \frac{[Tu]}{[Tu(0)]} = -k_p t$	$-\frac{d[Tu]}{dt} = k_p[Tu]$
$\ln \frac{[MT]}{[MT(0)]} = -(k_d + k_t[tau(t)])t$	$-\frac{d[MT]}{dt} = \overline{k}_d[MT]$

Table A.6: First-order kinetic equations describing MTs polymerization and depolymerization.

This model is definitely more detailed than the one used in this work, but unfortunately the lack of the parameter values didn't make possible its use.
Another model, cited in Chapter 2, considered as a possible substitute for the one just described is that by Marx and Mendelkow in 1994[32]. It consists in a more complex and detailed system that the Dogterom-Leibler's one, where the polymerization kinetics of microtubules is described with seven differential equations, each of which represents a phase in the reaction cycle.

$$
\begin{aligned}
&(1)\ \dot{c}_G = k_{nuc} - k_{cat}\, c_G + k_{resc}\, c_S \\
&(2)\ \dot{c}_S = k_{cat}\, c_G - k_{resc}\, c_S - k_{depol} \frac{c_S^2}{c_{shr}} \\
&(3)\ \dot{c}_{shr} = k_{cat}\, c_{grw} - k_{resc}\, c_{shr} - k_{depol}\, c_S \\
&(4)\ \dot{c}_{oli} = k_{depol}\, c_S - k_{oli}\, c_{oli} \\
&(5)\ \dot{c}_{ina} = k_{oli}\, c_{oli} - k_{exc}\, c_{exc} \\
&(6)\ \dot{c}_{act} = k_{exc}\, c_{exc} - (k_+ c_{act} - k_-) c_G \\
&(7)\ \dot{c}_{GTP} = -k_{spon}\, c_{GTP} - k_{exc}\, c_{exc}
\end{aligned}
$$

with:

$$
k_{nuc} := q_{nuc} \exp\left(\frac{c_{eff} - z_{nuc}}{s_{nuc}}\right) \qquad c_{eff} := c_{act} \exp(-g(c_{oli} + c_{ina}))
$$

$$
k_{cat} := q_{cat} \exp\left(\frac{z_{cat} - c_{eff}}{s_{cat}}\right) \qquad c_{exc} := c_{ina} - \frac{c_{act} + c_{ina}}{r \dfrac{c_{GTP}}{c_{GXP} - c_{GTP}} + 1}
$$

$$
c_{grw} := c_{tot} - c_{oli} - c_{ina} - c_{act} - c_{shr}
$$

Figure A.1: MTOSC system of differential equations.

Another work, where a model of MTs dynamic instability is proposed, is the dissertation by Frederick Laud Amoah-Darko Jr. for Clarkson University[44]. He describes the previous works already present, and then proceeds to develop his own.

Appendix B

Parameter values

In Appendix A, it has been said that the first kinetic model developed couldn't be used due to a lack of parameter values, but, other than that, another difficulty was to link the few values available together, as these were also dimentionally different.

However, it is important to collect all the available data to help future researcher to continue this work and manage to reach the goals mentioned for the future studies.

Here listed below, are the parameter values collected for the kinetic model:

Kinetic Constant	**Value**
k_1[GSK3β]	$9.63{\cdot}10^{-5}$
k_2	/
k_3	/
k_4	11.6μM
k_5	/
k_6	$6.13{\cdot}10^{-5}$ - $4.17{\cdot}10^{-26}$ [20]
k_7	/
k_8	/
k_{NFT}	$19.2{\cdot}10^{-11}$ μg/(mL·s)
k_p	$90s^{-1}$[45]
k_d	$70s^{-1}$[45]
k_t	/

Table B.1: Reaction rates k of the equation listed in Appendix A. These values depend on experimental conditions.

It can be seen that in **Table B.1** and **Table B.2** many values are not available, and the reasons for this is that experiments are usually conducted in different conditions or with different hypothesis, so it is hard to find numbers that correlates between one another.

Concentration	**Value**	**Initial Concentration**	**Value**
$[tau]$	$7.7{\cdot}10^{10}$pg (healthy) $1.14{\cdot}10^{11}$pg (AD)	[tau(0)]	/
$[GSK3\beta]$	/	$[GSK3\beta(0)]$	/
$[CaMKII]$	/	[CaMKII(0)]	/
$[CDK1]$	/	[CDK1(0)]	/
$[tau^*]$	/	$[tau^*(0)]$	/
$[PP2A]$	/	[PP2A(0)]	/
$[MT]$	/	[MT(0)]	/
$[MT^*]$	/	$[MT^*(0)]$	/
$[Tu]$	/	[Tu(0)]	130μM[45]

Table B.2: Concentrations of compounds listed in Appendix A. These values are referred to the entire brain.

In order to find more data that could be useful, the open access resource Human Protein Atlas (HPA) was explored. This database was created with the goal of mapping human proteins and genes in cells, tissues and organs through the integration of omics technologies.
Here, the data are referred as transcript par million (TPM), which represent the number of transcripts for a given gene. Another measure is the normalized TPM (nTPM), which considers the values from more than one database proceeding then with a normalizing operation. Moreover, the normalized TPM is proportional to the relative RNA molar concentration (rmc). Listed in **Table B.3**, there are the values of RNA expression collected from HPA.

	RNA expression
Tau	135.5 nTPM
GSK3β	20.6 nTPM
CaMKIIα	421.5 nTPM
CaMKIIβ	87.7 nTPM
CDK1	2.1 nTPM

Table B.3: Values of RNA expression collected from HPA.

Some other data have been collected by Marx and Mendelkow for their model, published in 1994[32], consisting in a more detailed system of equations describing MTs dynamic instability.

Table 2. Parameters used in numerical simulations and comparison with experimental data

	Units	Simulations			Experiments	
		MT-prot., osc. buff. (Fig. 2)	PC-tubulin, osc. buff. (Fig. 3a)	PC-tubulin, reass. b. (Fig. 3b)	plus ends	minus ends
k_+	$\mu M^{-1} s^{-1}$	15	15	10	7 (11)[b]	4 (5)[b]
k_-	s^{-1}	120	120	45	43 (89)[b]	25 (33)[b]
k_{depol}	s^{-1}	8000	8000	800	800 (8000)[b]	840 (8000)[b]
q_{cat}	s^{-1}	0.00015	0.00015	0.00008	--	--
z_{cat}	μM	80	80	80	--	--
s_{cat}	μM	10	10	10	4–13[c]	4–13[c]
k_{resc}	s^{-1}	0.2	0.2	0.4	0.08 (0.09)[b]	0.36 (0.17)[b]
g	μM^{-1}	0.021	0.008	0.008	--	--
q_{nuc}	$\mu M^{-1} s^{-1}$	0.00012	0.00012	0.00012	--	
z_{nuc}	μM	60	60	60	--	
s_{nuc}	μM	60	60	60	--	
k_{oligo}	s^{-1}	0.04	0.04	4[a]	$\approx$0.02[d]	
k_{exc}	s^{-1}	0.08	0.08	0.08	0.1–0.2[e]	
r	1	2	2	2	1.9–2.5[f]	
k_{spon}	s^{-1}	0.0003	0.001	0.001	--	

[a] Oligomers are discarded from the reaction cycle by choosing a very high dissociation rate
[b] Obermann-Pleß (1992); results obtained by dark-field microscopy of single MTs at tubulin concentrations in the range from 1.3 to 3.8 mg/ml. Values in parentheses are measured in oscillation buffer (0.1 M PIPES pH 6.9, containing 4 mM GTP, 20 mM $MgCl_2$, and 60 mM NaCl), other values in standard reassembly buffer (0.1 M PIPES pH 6.9, containing 1 mM GTP and 1 mM $MgSO_4$)
[c] Walker et al. (1988, 1991)
[d] Melki et al. (1988, 1989); the rate depends on buffer conditions (e.g. concentration of Mg^{++}) and protein composition (MAPs)
[e] Engelborghs and Eccleston (1982); Melki et al. (1988, 1989)
[f] Martin and Bayley (1987)

Figure B.1: Parameter values used in Marx-Mendelkow model.[32]

Moreover, Frederick Laud Amoah-Darko Jr's dissertation for Clarkson University [44]contains the parameter values he used in his model, which also are the starting set for the variation he considered in his analysis.

Parameter	SI units	Baseline value
p_c	μM	2
$p(0)$	μM	15
α	μm min$^{-1}\mu$M^{-1}	2.5
γ^h	μm min^{-1}	6
C	min^{-1}	0 or 0.1
N_{tr}	dimensionless	0 or 1.5
δ	μm min^{-1}	20
λ	min^{-1}	0.136
μ	M^{-1}min^{-1}	5.9×10^3
κ	min^{-1}	1
L	μm	20 or 40

Figure B.2: Basecase model parameters for simulations.

Bibliography

[1] M. Calabrò, C. Rinaldi, G. Santoro, and C. Crisafulli. «The biological pathways of Alzheimer disease: a review». In: *AIMS Neuroscience* 8 (1 2021), pp. 86–132. ISSN: 23737972. DOI: 10.3934/Neuroscience.2021005 (cit. on p. 1).

[2] A. Delacourte and A. Defossez. *Alzheimer's Disease: Tau Proteins, the Promoting Factors of Microtubule Assembly, are Major Components of Paired Helical Filaments*. 1986 (cit. on p. 1).

[3] E. Karran, M. Mercken, and B. De Strooper. *The amyloid cascade hypothesis for Alzheimer's disease: An appraisal for the development of therapeutics*. Sept. 2011. DOI: 10.1038/nrd3505 (cit. on p. 1).

[4] X. Zhang, Z. Fu, L. Meng, M. He, and Z. Zhang. *The Early Events That Initiate β-Amyloid Aggregation in Alzheimer's Disease*. Nov. 2018. DOI: 10.3389/fnagi.2018.00359 (cit. on p. 2).

[5] M. R. Brown, S. E. Radford, and E. W. Hewitt. *Modulation of β-Amyloid Fibril Formation in Alzheimer's Disease by Microglia and Infection*. Nov. 2020. DOI: 10.3389/fnmol.2020.609073 (cit. on p. 2).

[6] A. A. Kulikova, A. A. Makarov, and S. A. Kozin. *Roles of zinc ions and structural polymorphism of β-amyloid in the development of Alzheimer's disease*. Mar. 2015. DOI: 10.1134/S0026893315020065 (cit. on p. 2).

[7] S. I. A. Cohen et al. «Proliferation of amyloid-β42 aggregates occurs through a secondary nucleation mechanism». In: *Proceedings of the National Academy of Sciences of the United States of America* 110 (24 June 2013), pp. 9758–9763. ISSN: 00278424. DOI: 10.1073/pnas.1218402110 (cit. on p. 2).

[8] C. Piller. «Research backing experimental Alzheimer's drug was first target of suspicion». In: *Science* 377.6604 (2022), pp. 363–363. DOI: 10.1126/science.ade0181 (cit. on p. 2).

[9] F. Kametani and M. Hasegawa. *Reconsideration of amyloid hypothesis and tau hypothesis in Alzheimer's disease*. Jan. 2018. DOI: 10.3389/fnins.2018.00025 (cit. on p. 2).

[10] P. Barbier, O. Zejneli, M. Martinho, A. Lasorsa, V. Belle, C. Smet-Nocca, P. O. Tsvetkov, F. Devred, and I. Landrieu. *Role of tau as a microtubule-associated protein: Structural and functional aspects*. 2019. DOI: 10.3389/fnagi.2019.00204 (cit. on pp. 3, 12).

[11] H. Yadikar, I. Torres, G. Aiello, M. Kurup, Z. Yang, F. Lin, F. Kobeissy, R. Yost, and K. K. Wang. «Screening of tau protein kinase inhibitors in a tauopathy-relevant cell-based model of tau hyperphosphorylation and oligomerization». In: *PLoS ONE* 15 (7 July July 2020). ISSN: 19326203. DOI: 10.1371/journal.pone.0224952 (cit. on p. 3).

[12] J. Avila, J. S. Jiménez, C. L. Sayas, M. Bolós, J. C. Zabala, G. Rivas, and F. Hernández. *Tau Structures*. Nov. 2016. DOI: 10.3389/fnagi.2016.00262 (cit. on p. 3).

[13] D. Wang, X. Huang, L. Yan, L. Zhou, C. Yan, J. Wu, Z. Su, and Y. Huang. *The Structure Biology of Tau and Clue for Aggregation Inhibitor Design*. Oct. 2021. DOI: 10.1007/s10930-021-10017-6 (cit. on p. 4).

[14] K. Iqbal et al. *Tau pathology in Alzheimer disease and other tauopathies*. Jan. 2005. DOI: 10.1016/j.bbadis.2004.09.008 (cit. on pp. 5, 6).

[15] R. Medeiros, D. Baglietto-Vargas, and F. M. Laferla. *The Role of Tau in Alzheimer's Disease and Related Disorders*. Oct. 2011. DOI: 10.1111/j.1755-5949.2010.00177.x (cit. on p. 5).

[16] H. C. Cheng, R. Z. Qi, H. Paudel, and H. J. Zhu. *Regulation and function of protein kinases and phosphatases*. 2011. DOI: 10.4061/2011/794089 (cit. on p. 7).

[17] L. Martin, X. Latypova, C. M. Wilson, A. Magnaudeix, M. L. Perrin, C. Yardin, and F. Terro. *Tau protein kinases: Involvement in Alzheimer's disease*. Jan. 2013. DOI: 10.1016/j.arr.2012.06.003 (cit. on pp. 7–9).

[18] J. Z. Wang, Q. Wu, A. Smith, I. Grundke-Iqbal, and K. Iqbal. «τ is phosphorylated by GSK-3 at several sites found in Alzheimer disease and its biological activity markedly inhibited only after it is prephosphorylated by A-kinase». In: *FEBS Letters* 436 (1 Sept. 1998), pp. 28–34. ISSN: 00145793. DOI: 10.1016/S0014-5793(98)01090-4 (cit. on p. 7).

[19] M. Oka, N. Fujisaki, A. Maruko-Otake, Y. Ohtake, S. Shimizu, T. Saito, S. I. Hisanaga, K. M. Iijima, and K. Ando. «Ca2+/calmodulin-dependent protein kinase II promotes neurodegeneration caused by tau phosphorylated at Ser262/356 in a transgenic Drosophila model of tauopathy». In: *Journal of Biochemistry* 162 (5 Nov. 2017), pp. 335–342. ISSN: 17562651. DOI: 10.1093/jb/mvx038 (cit. on p. 8).

[20] T. J. A. Craddock, J. A. Tuszynski, and S. Hameroff. «Cytoskeletal signaling: Is memory encoded in microtubule lattices by CaMKII phosphorylation?» In: *PLoS Computational Biology* 8 (3 2012). ISSN: 15537358. DOI: 10.1371/journal.pcbi.1002421 (cit. on pp. 8, 56).

[21] L. Clementi, S. Sabetta, V. Zelli, C. Compagnoni, A. Tessitore, V. Mattei, and A. Angelucci. «Mitotic phosphorylation of Tau/MAPT modulates cell cycle progression in prostate cancer cells». In: *Journal of Cancer Research and Clinical Oncology* 149 (10 Aug. 2023), pp. 7689–7701. ISSN: 14321335. DOI: 10.1007/s00432-023-04721-2 (cit. on p. 8).

[22] L. Martin, X. Latypova, C. M. Wilson, A. Magnaudeix, M. L. Perrin, and F. Terro. *Tau protein phosphatases in Alzheimer's disease: The leading role of PP2A*. Jan. 2013. DOI: 10.1016/j.arr.2012.06.008 (cit. on p. 8).

[23] Santanu Mukherjee. *Microtubules: Definition, location, structure, functions*. Feb. 2023. URL: https://www.sciencefacts.net/microtubules.html (cit. on p. 11).

[24] P. W. Baas, A. N. Rao, A. J. Matamoros, and L. Leo. *Stability properties of neuronal microtubules*. Sept. 2016. DOI: 10.1002/cm.21286 (cit. on p. 11).

[25] G. J. Brouhard and L. M. Rice. *Microtubule dynamics: An interplay of biochemistry and mechanics*. July 2018. DOI: 10.1038/s41580-018-0009-y (cit. on p. 12).

[26] R. H. Wade. *On and around microtubules: An overview*. Oct. 2009. DOI: 10.1007/s12033-009-9193-5 (cit. on p. 12).

[27] P. Hinow, V. Rezania, and J. A. Tuszyński. «Continuous model for microtubule dynamics with catastrophe, rescue, and nucleation processes». In: *Physical Review E - Statistical, Nonlinear, and Soft Matter Physics* 80 (3 Sept. 2009). ISSN: 15393755. DOI: 10.1103/PhysRevE.80.031904 (cit. on pp. 12, 16).

[28] C. Conde and A. Cáceres. *Microtubule assembly, organization and dynamics in axons and dendrites*. May 2009. DOI: 10.1038/nrn2631 (cit. on p. 12).

[29] B. Li, M. O. Chohan, I. Grundke-Iqbal, and K. Iqbal. «Disruption of microtubule network by Alzheimer abnormally hyperphosphorylated tau». In: *Acta Neuropathologica* 113 (5 May 2007), pp. 501–511. ISSN: 00016322. DOI: 10.1007/s00401-007-0207-8 (cit. on p. 13).

[30] R. Dhamodharan and P. Wadsworth. «Modulation of microtubule dynamic instability in vivo by brain microtubule associated proteins». In: *Journal of Cell Science* 108.4 (Apr. 1995), pp. 1679–1689. ISSN: 0021-9533. DOI: 10.1242/jcs.108.4.1679 (cit. on p. 14).

[31] M. Dogterom and S. Leibler. *Physical Aspects of the Growth and Regulation of Microtubule Structures Microtubules (MTs) are long, rigid polymers made of tubulin-a globular protein found in eukaryotic cells [1].* 1993 (cit. on pp. 14, 27).

[32] A. Marx and E. Mandelkow. *European Biophysics Journal A model of microtubule oscillations.* 1994 (cit. on pp. 18, 53, 58).

[33] E. M. Mandelkow, G. Lange, A. Jagla, U. Spann, and E. Mandelkow. «Dynamics of the microtubule oscillator: role of nucleotides and tubulin-MAP interactions.» In: *The EMBO journal* 7 (2 1988), pp. 357–365. ISSN: 02614189. DOI: 10.1002/j.1460-2075.1988.tb02821.x (cit. on p. 18).

[34] H. Bolterauer, H. J. Limbach, and J. A. Tuszynski. *Models of Assembly and Disassembly of Individual Microtubules: Stochastic and Averaged Equations.* 1999 (cit. on p. 18).

[35] S. Herculano-Houzel. *The human brain in numbers: A linearly scaled-up primate brain.* Nov. 2009. DOI: 10.3389/neuro.09.031.2009 (cit. on p. 19).

[36] F. A. C. Azevedo, L. R. B. Carvalho, L. T. Grinberg, J. M. Farfel, R. E. L. Ferretti, R. E. P. Leite, W. J. Filho, R. Lent, and S. Herculano-Houzel. «Equal numbers of neuronal and nonneuronal cells make the human brain an isometrically scaled-up primate brain». In: *Journal of Comparative Neurology* 513 (5 Apr. 2009), pp. 532–541. ISSN: 00219967. DOI: 10.1002/cne.21974 (cit. on p. 19).

[37] D. G. T. Barrett, S. Denève, and C. K. Machens. «Optimal compensation for neuron death». In: (). DOI: 10.1101/029512. URL: https://doi.org/10.1101/029512 (cit. on p. 19).

[38] J. Wegiel et al. «Clinicopathological staging of dynamics of neurodegeneration and neuronal loss in Alzheimer disease». In: *Journal of Neuropathology and Experimental Neurology* 80 (1 2021), pp. 21–44. ISSN: 15546578. DOI: 10.1093/JNEN/NLAA140 (cit. on pp. 19, 21, 22).

[39] M. H. Toft, O. Gredal, and B. Pakkenberg. *The size distribution of neurons in the motor cortex in amyotrophic lateral sclerosis.* 2005 (cit. on p. 23).

[40] L. Congiu. «Computational investigations of the link between hyperphosphorylation of MAP tau and melatonin binding in Alzheimer's disease». MA thesis. Politecnico di Torino, 2023 (cit. on p. 25).

[41] R. L. Best, N. E. LaPointe, J. Liang, K. Ruan, M. F. Shade, L. Wilson, and S. C. Feinstein. «Tau isoform–specific stabilization of intermediate states during microtubule assembly and disassembly». In: *Journal of Biological Chemistry* 294.33 (2019), pp. 12265–12280. ISSN: 0021-9258. DOI: https://doi.org/10.1074/jbc.RA119.009124 (cit. on p. 26).

[42] D. N. Drechsel, A. A. Hyman, M. H. Cobb, and M. W. Kirschner. *Modulation of the Dynamic Instability of Tubulin Assembly by the Microtubule-Associated Protein Tau*. 1992 (cit. on p. 29).

[43] F. Pampaloni, G. Lattanzi, A. Jonáš, T. Surrey, E.n Frey, and E. L. Florin. «Thermal fluctuations of grafted microtubules provide evidence of a length-dependent persistence length». In: *Proceedings of the National Academy of Sciences* 103.27 (2006), pp. 10248–10253. DOI: 10.1073/pnas.0603931103 (cit. on p. 35).

[44] F. Laud Amoah-Darko and D. White. «Modeling microtubule dynamic instability: Microtubule growth, shortening and pause». In: *Journal of Theoretical Biology* 553 (Nov. 2022). ISSN: 10958541. DOI: 10.1016/j.jtbi.2022.111257 (cit. on pp. 54, 59).

[45] T. J. A. Craddock, J. A. Tuszynski, D. Chopra, N. Casey, L. E. Goldstein, S. R. Hameroff, and R. E. Tanzi. «The zinc dyshomeostasis hypothesis of Alzheimer's disease». In: *PLoS ONE* 7 (3 Mar. 2012). ISSN: 19326203. DOI: 10.1371/journal.pone.0033552 (cit. on pp. 56, 57).